



# Grain size dependent large rheology contrasts of halite at low deviatoric stress: evidence from microstructural study of naturally deformed gneissic Zechstein-2 rock salt (Kristallbrockensalz) from the Northern Netherlands

5 Jessica Barabasch<sup>1</sup>, Joyce Schmatz<sup>2</sup>, Jop Klaver<sup>2</sup>, Alexander Schwedt<sup>3</sup>, Janos L. Urai<sup>1</sup>

<sup>1</sup> Institute for Structural Geology, Tectonics and Geomechanics, RWTH Aachen University, Lochnerstrasse 4-20, D-52056 Aachen, Germany

<sup>2</sup> MaP – Microstructure and Pores GmbH, Junkerstrasse 93, 52064 Aachen, Germany

<sup>3</sup> Central Facility for Electron Microscopy (GFE), RWTH Aachen University.

10 *Correspondence to:* Jessica Barabasch (Jessica.barabasch@emr.rwth-aachen.de)

**Abstract.** Constitutive laws of rock salt are required for the prediction of long-term deformation of radioactive waste repositories and solution mined caverns, which are used for energy storage and play an important role in the energy transition. Much of this deformation is at differential stresses of a few MPa. The vast majority of laboratory measurements of salt creep are at much higher differential stress and require extrapolation over many orders of magnitude. This extrapolation can be made more reliable by including microphysical information on the deformation mechanisms in the laboratory samples, integrated with microstructural analysis of samples deformed in natural laboratories at low differential stress.

20 Rock salt can deform at widely different rates at the same temperature and deviatoric stress, depending on state variables such as grain size, solid solution- and second phase- impurities, crystallographic preferred orientation, water content and grain boundary structure. Both dislocation creep and dissolution-precipitation creep processes are common, but dissolution-precipitation creep (pressure solution) is not commonly included in current engineering predictions.

Here we show evidence for large grain size-dependent differences in halite rheology based on microstructural observations from Zechstein rock salt cores of the Northern Netherlands that experienced different degrees of tectonic deformation. We studied the relatively undeformed Z2 (Stassfurt Formation), horizontal-layered salt from Barradeel, and compare it with much stronger deformed equivalent in diapiric salt form Winschoten, Zuidwending, and Pieterburen. We used optical microscopy of Gamma-irradiated thin sections for microtectonic analysis, recrystallized grain size measurements and subgrain size piezometry, SEM-EDX and XRD for second phase mineralogy. Subgrain size piezometry shows that this deformation took place at differential stress between 0.5 and 2 MPa, providing a natural laboratory.

30 In the undeformed, layered salt from Barradeel we find cm-thick layers of single crystalline halite (Kristalllagen) alternating with fine-grained halite and thin anhydrite layers. The domal salt samples are typical of the well-known "Kristallbrocken" salt, and consist of cm-size tectonically disrupted megacrystals surrounded by fine-grained halite with grain size of a few



mm. We infer high strains in the fine-grained halite as shown by folding and boudinage of thin anhydrite layers, as compared to the megacrystals, which are internally much less deformed and develop subgrains during dislocation creep. Subgrain size shows comparable differential stresses in Kristallbrocken than in matrix salt. The fine-grained matrix salt is dynamically recrystallized, has few subgrains and microstructures indicating deformation by solution-precipitation processes. We infer that the finer grained halite deformed dominantly via pressure solution and the megacrystals dominantly by dislocation creep.

This provides evidence that the fine-grained matrix salt is much weaker than Kristallbrocken because of different dominant deformation mechanisms. This is in agreement with microphysical models of pressure solution creep in which grain size has a significant effect on strain rate at these low differential stress. Our results on the operation of pressure solution creep in rock salt at differential stress of a few MPa point to the importance of this mechanism at low differential stresses around engineered structures but also in most salt tectonic settings. We suggest that including results of microstructural analysis can strongly improve engineering models of rock salt deformation.

We recommend that this mechanism of grain size dependent rheology is included more consistently in the constitutive laws describing deformation of engineered structures in rock salt.

## 1 Introduction

### 1.1 Salt rheology, deformation processes and associated microstructures - relevance of natural laboratories

Salt - unlike most sedimentary rocks - is very weak and deforms like a viscous fluid, even at low temperatures and shallow depths, and its presence in sedimentary basins fundamentally changes their evolution by salt tectonic processes (Jackson et al., 1994; Urai et al., 2008; Jackson and Hudec, 2017). This has long been recognized for salt diapirs, (Trusheim, 1957; Schultz-Ela et al., 1993; Kukla et al., 2019), salt glaciers (Wenkert, 1979; Talbot, 1979; Talbot and Aftabi, 2004; Závada et al., 2012), salt decoupling (Peel, 2014; Rowan and Krzywiec, 2014; Tămaş et al., 2021), and at a smaller scale for internal salt flow creating folding or boudinage (van Gent et al., 2011; Fiduk and Rowan, 2012; Strozyk et al., 2014; Dooley et al., 2015; Rowan et al., 2019; Adamuszek et al., 2021).

Rock salt is the host of many large engineering constructions like salt caverns and radioactive waste repositories and the long-term operation of these structures requires predictions of deformation up to thousands of years (Brouard et al., 2004; Chemia et al., 2009; Bräuer et al., 2011; Baumann et al., 2018). This deformation takes place at differential stresses of below a few MPa, however the measurement of salt rheology in the laboratory is problematic because of the long duration of the required experiments (Brouard et al., 2004; Bérest et al., 2010). Because laboratory experiments are limited in time, they are commonly conducted at relatively high deviatoric stresses and strain rates at which dislocation creep processes are expected and inferred to be the dominant deformation mechanism (Wawersik and Zeuch, 1986; Carter et al., 1993; Hunsche and Hampel, 1999; Hampel et al., 2007; Urai and Spiers, 2007; Urai et al., 2008; Hampel, 2016). Therefore, most of the long term predictions of salt deformation have been made based on extrapolation of such experimentally derived power-law creep



65 rheology to low differential stress (Albrecht et al., 1993; Bräuer et al., 2011), although some predictions include both mechanisms (Buijze et al., 2022). However, it has been documented in the geological and materials science literature that below a certain differential stress in rock salt there can be a grain size-dependent dramatic change in deformation mechanism from dislocation creep to pressure solution creep and this can change the creep rate by many orders of magnitude (Urai et al., 1986b; Spiers et al., 1990; van Keken et al., 1993; Spiers and Carter, 1998).

70 In recent years, the validity of dislocation creep-based extrapolations was extensively discussed in the engineering community, and very slow creep tests were carried out that indeed show much faster deformation than power law creep rates would predict (Popp and Hansen, 2018; Bérest et al., 2019).

An important contribution to this discussion comes from materials science, where microphysical processes are related to constitutive laws by state variables such as water content (at grain boundaries), solid solution and second phase impurities and grain size (Carter and Hansen, 1983; Heard and Ryerson, 1986; Urai et al., 1986b; Hunsche et al., 2003; Bérest et al., 2019; Spiers et al., 1990). For steady state and non-dilatant deformation the microphysics-based deformation rate of rock salt is given by following Eq. (1):

$$\dot{\epsilon}_{DC} = Ae^{-\frac{Q_{DC}}{RT}} (\sigma_1 - \sigma_3)^n, \quad (1)$$

for dislocation creep, and Eq. (2):

80 
$$\dot{\epsilon}_{PS} = Be^{-\frac{Q_{PS}}{RT}} \left( \frac{\sigma_1 - \sigma_3}{D^m} \right), \quad (2)$$

for solution-precipitation creep, with the sum of both being the total strain rate Eq. (3):

$$\dot{\epsilon} = \dot{\epsilon}_{PS} + \dot{\epsilon}_{DC}, \quad (3)$$

(Wawersik and Zeuch, 1986; Spiers et al., 1990; Carter et al., 1993; van Keken et al., 1993; Hunsche and Hampel, 1999; Urai et al., 2008). Thereby A and B are material constants,  $Q_{DC}$  and  $Q_{PS}$  are apparent activation energies for dislocation creep and pressure-solution creep,  $R$  is the gas constant,  $T$  is absolute temperature,  $\sigma_1 - \sigma_3$  is the differential stress,  $D$  is the grain size and  $n$  and  $m$  are stress and grain size exponents. For a compilation of parameters for the two mechanisms, we refer to Urai et al., 2008 and references therein (e.g. Spiers et al., 1990; van Keken et al., 1993; Brouard and Bérest, 1998; Hunsche and Hampel, 1999; Hunsche et al., 2003).

Because of the large differences in the stress and grain size exponents of the two mechanisms, pressure solution creep will dominate deformation at low differential stress and small grain size and dislocation creep will dominate deformation at high differential stress and large grain size. Key parameters in the evolution of grain size are the structure and mobility of brine-filled grain boundaries, which can change as a function of differential stress (Drury and Urai, 1990; van Noort et al., 2008); and the migration of grain boundaries, which can change the grain size (Urai et al., 1986a; Peach et al., 2001; Schenk and Urai, 2004; Schenk et al., 2006; Schmatz et al., 2011).



95 Because of the extremely long experiments (several years) required to measure pressure solution creep rates in rock salt  
(Bérest et al., 2019) and the very small strains reached in these experiments, it is useful to compare these results with  
naturally deformed samples. The differential stresses during natural deformation can be measured using subgrain size  
piezometry and are commonly found to be between 0.5 and 5 MPa (Carter et al., 1982; Schlöder and Urai, 2005; Leitner et  
al., 2011; Rowan et al., 2019), but to much higher strains than can be achieved in low stress laboratory experiments. In  
100 addition, relative differences in rheology can be measured in layered salt (Talbot, 1979; Carter et al., 1982; Schmalholz and  
Podladchikov, 2001; Schlöder and Urai, 2005; Hudleston and Treagus, 2010; Leitner et al., 2011; Komoróczy et al., 2013;  
Zulauf et al., 2014; Závada et al., 2015; Schmalholz and Mancktelow, 2016; Adamuszek et al., 2021; Schlöder and Urai,  
2007). Microstructural observations of naturally deformed samples show that dislocation creep, dynamic recrystallization  
and pressure solution creep can be readily distinguished, indicated by plastic crystal deformation forming slip bands and  
105 subgrains (dislocation creep), crystal overgrowth (dynamic recrystallization) as well as growth bands and crystal elongation  
(pressure solution creep) (Desbois et al., 2010, 2012; Závada et al., 2012, 2015).

## 1.2 Kristallbrocken- salt

The Kristallbrocken salt in the Zechstein II (Stassfurt Formation in Germany) is a well-known tectonite in the Permian  
Basin. Richter-Bernburg (1953) described *Trümmersalze* (German: ‘Trümmersalze’ = debris salt) with Kristallbrocken  
110 (German: ‘Kristallbrocken’ = crystal fragments) salt as large, sharp-edged crystal porphyroblasts inside a fine recrystallized  
matrix (Küster et al., 2008). Vintage mine photographs from Northern Germany show layer-parallel boudins of  
Kristallbrocken, large rotations of fragments and regular boudinage in multiple 20 cm thick layers (Richter-Bernburg, 1953;  
Simon, P., 1972). It is interpreted to have formed out of a **layer cake of fine-grained matrix salt**, layers of single crystalline  
halite (German: ‘*Kristalllagen*’ = crystal layer (Seidl, 1914)), and thin anhydrite layers by deformation, resulting in an  
115 augengneiss structure, with the Kristallbrocken decreasing in size with tectonic strain (Küster et al., 2008, 2009; Urai et al.,  
2019). Pape et al., (2002) presented samples from the Gorleben salt dome and showed that the depositional setting of  
‘Kristalllagen’ halite was shallow marine based on the occurrence of abundant fluid inclusion trails in chevron patterns.  
Another argument for Kristallbrocken being fragments from a primary layering is based on observations of internal  
laminations of fluid and solid inclusions (Richter-Bernburg, 1953; Simon, P., 1972; Pape et al., 2002). Following earlier  
120 interpretations, (Richter-Bernburg, 1953; Simon, P., 1972), Pape et al. (2002) hypothesized that rupturing of halite crystal  
layers is attributable to early diagenetic destruction of layers from subaquatic gliding. This is in contrast to other  
interpretations (Löffler, 1962) were the so-called Augensalz (another name for Kristallbrockensalz) is interpreted to have  
formed from rupturing of halite crystal layers during tectonic flow, with clear halite crystallizing in the boudin necks.  
Extensive studies of distribution of bromide content, Kristallbrocken texture and microstructure, abundant sulphate and fluid  
125 inclusions in Kristallbrocken and interpretation of their formation and deformation mechanisms were presented by Küster et  
al. (2008, 2009, 2011; Küster, 2011). The structural characteristics of the Kristallbrocken salt were attributed to brittle  
deformation, dislocation glide and a strong competence contrast between porphyroclastic Kristallbrocken salt and fine-



grained mylonitic matrix halite (Küster et al., 2010). Küster et al. (2009) described the matrix halite and inferred a dynamically recrystallized microstructure of sub-structured and sub-structure free grains. Lobate grain boundaries were interpreted to have formed by grain boundary migration recrystallization and it was later stated that due to the lack of crystallographic preferred orientation and high water contents fluid assisted solution-precipitation creep or grain boundary migration might have been dominant deformation mechanisms (pg. 139 in Küster, 2011). It was hypothesized that second phase inclusions, large grain size and the monocrystallinity of Kristallbrocken contribute to the observed rheology contrasts (Küster et al., 2008). In a more recent report from the KEM-17 study (Urai et al., 2019) boudinaged and folded anhydrite layers as well as boudinaged Kristallbrocken surrounded by recrystallized halite and original fine-grained halite were described in Zuidwending and Winschoten samples.

### 1.3 Aim of the study

In this study we build on the observations briefly reviewed above, and add our new observations on samples with Kristalllagen and Kristallbrocken from the Zechstein of the Netherlands (Fig. 1), and hypothesize that the large competence contrast and different deformation styles between Kristallbrocken and fine-grained matrix is caused by the different microphysical deformation mechanisms, with dislocation creep and ductile rupturing (boudinage) being dominant in the Kristallbrocken, and grain size dependent pressure solution creep being dominant in the fine-grained matrix. If this hypothesis is supported by our data, it provides further evidence for the operation of grain size-dependent creep in rock salt at the conditions relevant for the operation of engineered structures in rock salt.

## 2 Materials and Methods

We studied 21 samples from drill cores from the areas of Barradeel (BAS), Pieterburen (PBN), Zuidwending (ZW) and Winschoten (WSN, near Heiligerlee) Zechstein salt structures (Fig. 1). BAS, ZW and WSN samples were collected and prepared for the KEM-17 study without gamma irradiating them (Urai et al., 2019). The samples were selected in the TNO central core storage facility in Zeist and core shed of the mining company (BAS). They were cut perpendicular to the bedding in a dry laboratory with a diamond saw cooled by a small amount of slightly undersaturated salt brine to reduce mechanical damage (Schléder and Urai, 2005).

To decorate crystal defect structures in NaCl, samples were irradiated in the research reactor FRM-II at the TU Munich in Garching with varying dose rates between 6 and 11 kGy h<sup>-1</sup> to a total dose of 4 MGy at a constant temperature of 100 °C (Urai et al., 1986b; Garcia Celma et al., 1988; Schléder and Urai, 2005, 2007). Thin sections of un-irradiated samples were dry-polished to a thickness of approximately 1 mm, and gamma-irradiated thin sections were dry-polished to a thickness of approximately 50 µm to reach optical transparency. To decorate grain boundaries and subgrain boundaries, the samples were chemically etched with slightly undersaturated brine which was removed with a jet of n-hexane using the technique described in (Spiers et al., 1986; Urai et al., 1987). The thin sections were imaged in reflected and transmitted light using a



Zeiss optical microscope (Axioscope) with the stitching panorama function of the ZEN imaging software. Reflected light  
160 panoramas with 25x magnification were used for grain boundary digitization (Fig. 3,7) after making sure that the grain size  
distribution is sufficiently well captured.

Halite grain and subgrain boundaries were manually traced with a touch pen and tablet for statistical analysis. Grain and  
subgrain sizes for piezometry were analyzed with Fiji (Schindelin et al., 2012) and calculated as equivalent circular diameter  
(Schléder and Urai, 2005; Lopez-Sanchez and Llana-Fúnez, 2015) and differential stresses  $\sigma$  were calculated as follows  
165 according to (Carter et al., 1993; Schlöder and Urai, 2005) with subgrain size =  $D$ , Eq. (4):

$$\sigma = 107 * D^{-0.87}, \quad (4)$$

Electron microscopy with energy dispersive X-ray spectroscopy (SEM-EDS) mapping has been used to identify the chemical  
composition and distribution of second phase impurities in halite. We used an Oxford Instruments X-Max 150 EDS system  
at the Institute of Structural Geology, Tectonics and Geomechanics (RWTH Aachen University) at 15 kV acceleration  
170 voltage. The samples were sputter-coated with approximately 7 nm of tungsten for conductivity.

Crystallographic orientations were measured by means of Electron Backscatter Diffraction on one thin section using a  
Symmetry EBSD camera by Oxford Instruments attached to a GeminiSEM 300 SEM by Carl Zeiss Microscopy. The  
measurement was performed at an acceleration voltage of 20 kV and a probe current of approximately 10nA. To avoid  
charging of the uncoated specimen, the analysis was performed in variable pressure mode using Nitrogen at a pressure of 30  
175 Pa in the sample chamber. In a first measurement series, approximately half of the entire thin section was scanned by 30  
small measurement areas with a step size of 20  $\mu\text{m}$ , which afterwards were manually merged to a large dataset, finally  
covering an area of approx. 1.8 cm x 3 cm. The central Kristallbrockensalz region was subsequently measured again with  
higher spatial resolution by four measurements using a step size of 5  $\mu\text{m}$ , which after merging covered an area of  
approximately 0.7 cm x 1.4 cm. All EBSD data were collected and indexed in “refined accuracy” mode with AZtec V 5.1 by  
180 Oxford Instruments. The final indexed datasets were further evaluated with OIM Analysis V 8.0 by Ametek-EDAX.

Prior to the electron microscopical investigations, the samples were freshly polished and etched again using the method  
described above, and coated with tungsten (in the case of the EDX measurements) or left uncoated (in the case of the EBSD  
measurements).

Qualitative XRD measurements to identify impurity content were performed on a Bruker D8 equipped with a graphite  
185 monochromator and a scintillation counter. Scans were measured with Cu-K $\alpha$  radiation.

## 3 Results

### 3.1 Barradeel samples

The Zechstein salt at Barradeel is sub-horizontally layered as seen on seismic (Strozyk et al., 2014; Barabasch et al., 2019)  
and has a total thickness of 800 m with a 580 m thick Z2 salt at a depth of up to 3 km based on well data (BAS-01, Kaart



190 boringen | NLOG, 2022). Salt cores have mostly sub-horizontal layering except for sample KS-15 where layering is vertical, indicating local folding, which is common in these settings (Fig. 2a, b).

The salt is layered with cm-scale milky to honey-colored halite layers interbedded with mm thick anhydrite bands (Fig. 2a). There are large variations in grain size of halite, with 1 to 5 cm thick single megacrystal layers (Kristalllagen) alternating with layers of fine-grained (about 3 mm) and very fine-grained (about 0.2 mm) halite layers (Fig. 2a, c).

195 Kristalllagen are clear or milky with internal laminae (Fig. 2a, b) due to variable content of fluid and solid inclusions of sulphate minerals (Fig. 2e) as previously described (Simon, P., 1972; Küster et al., 2011). The Kristalllagen have bedding perpendicular or inclined cleavage cracks without displacement of layering, the cracks presumably caused by drilling (Fig. 2a, c). However, in sample KS-15 the Kristalllage is displaced by a few mm along cracks next to small folds in anhydrite bands (Fig. 2b, d) which points to tectonic origin. Gamma decoration in Kristalllagen is mostly homogenous blue (Fig. 2c, 200 d), except for a few dark laminae which are interpreted as healed cracks in sample KS-07 that show the same orientation as an open crack in the same crystal. A Kristalllage in sample KS-07 has abundant slip bands oriented at 45 degrees to the cleavage crack, consistent with slip on the [110] system (Fig. 2c). Kristalllagen are subgrain-free as seen in reflected light on etched surfaces (Fig. 2c). In sample KS-16 (Fig. 3) microstructures are very similar, with thicker anhydrite laminae. Cellular structures formed by dark blue gamma decoration (Fig. 2e) locally coincide with barely visible subgrain boundaries on 205 etched surface (Supplement 1), but do not correspond to the abundant inclusions. Some megacrystals have single 1 mm large subgrains with small angle misorientation of slip bands and hopper crystal cores indicated by arrays of cubic fluid inclusions with fluid and gas bubbles (Supplement 1).

The fine- and very fine-grained halite grains are equigranular, in layers of two distinct grain sizes classes of fine-grained (about 3 mm) and very fine-grained (about 0.2 mm) (Fig. 2c, g, h, Supplements 1). Grain boundaries are slightly curved 210 forming 120° angles at triple junctions (Fig. 2f, h). In reflected light, etched surfaces show that the only porosity in the salt is that of isolated fluid inclusions in grain boundaries (Supplement 1). Fine-grained Halite grains have white cores and blue growth structures, visible through gamma decoration (Fig. 2c, g). Most grains have bright crystal cores with characteristic arrangement of cubic and chevron shaped fluid inclusion trails and abundant impurities (Fig. 2g).

The layers with very fine grain sizes are rich in dispersed anhydrite and polyhalite (0.1 to 1 mm) located usually at grain 215 boundaries (Fig. 2c, f, g, h).

Anhydrite layers of up to 5 mm thickness consist of  $\mu\text{m}$  to mm-sized anhydrite and polyhalite grains and occasionally include 0.1 to 1 mm sized halite crystals (Fig. 2c, d, g, h). These layers are straight or locally folded and continuous.

### 3.2 Diapiric salt samples from Pieterburen, Winschoten and Zuidwending

The studied Z2 rock salt comes from cores of 3 different salt diapirs (Winschoten (WSN), Zuidwending (ZW) and 220 Pieterburen (PBN) (Juez-Larré et al., 2019). Base salt reaches a depth of 3000 m and the salt pierces the overburden up to depths of 100 m as in the case of Zuidwending diapir (Geluk et al., 2007). The bedding as seen in core is mostly vertical,





strongly deformed with the older Z2 salt in the center, except for Pieterburen structure, where the younger salt is in the center (Geluk et al., 2007). The samples come from 260 m to 1800 m depth.

The deformed diapiric salt consists of Kristallbrocken, surrounded by fine-grained and very fine-grained matrix halite and folded or boudinaged anhydrite bands (Fig. 3) together with dispersed anhydrite and polyhalite inclusions, also confirmed by XRD measurements (Supplement 5). These inclusions locally have a lighter blue-colored halite rim but in the majority of cases the inclusions are not associated with color changes in the surrounding halite crystal. The rock salt has a typical gneissic appearance consistent with earlier descriptions of Kristallbrockensalz (Küster et al., 2008, 2011 and references in these).

The Kristallbrocken megacrystals are between 5 mm and 3 cm thick (comparable to the thickness of Kristalllagen in Barradeel) with a strongly elongated shape up to decimeters long (possibly longer but this could not be confirmed due to limitations of core dimensions (Fig. 4a-d). Kristallbrocken grains can be correlated to adjacent ones by thickness, inclusion content and crystallographic orientation (EBSD data, see below and Fig. 3, Fig. 4, Fig. 8). In a number of cases, Kristallbrocken can be seen to contain a fracture along which the two megacrystals are displaced, and in other cases the two megacrystals are boudinaged with the boudin necks filled with inclusion-free overgrowth on the megacrystals, or with fine-grained matrix halite in the boudin-neck (Fig. 3, Fig. 4).

A good example is presented in Figure 4d (BS-A), where two 1 cm thick Kristallbrocken parts can be correlated by thickness, enrichment of inclusions in the upper part and adjacent anhydrite bands. The 2 cm boudin neck contains epitaxially grown (see EBSD below), inclusion-free halite from both crystals and fine-grained halite matrix (Fig. 4d). Both inclusion-free overgrowths also have lighter blue gamma irradiation color. Two adjacent thin Anhydrite layers are also discontinuous, in coherence with the boudinaged Kristallbrocken. A 3 cm thick Kristallbrocken below is also displaced and has a small inclusion-free overgrowth. Both inclusion-free parts of the crystal also have lighter blue gamma irradiation color.

Gamma-decorated slip bands and subgrains are present in all Kristallbrocken, visible as white or dark blue subgrain boundaries and in reflected light on etched surfaces (Fig. 5a, Supplements 2). Subgrain sizes are on average 100 to 200 µm (Table 1) and subgrains can be either rounded or elongated with preferred orientation of subgrain boundaries forming a subgrain boundary network. Figure 5d shows one of the interpreted subgrain networks together and Table 1 shows the subgrain size statistics of all samples. Images of all other samples are included in the Supplement 2, together with their interpretation and subgrain size distribution. An interesting aspect of the subgrain boundary network is their locally fibrous morphology in the overgrowths in boudin-necks, these are interpreted as grown-in subgrains (Fig. 8) (Is and Ree, 1988).

Planar arrays of fluid inclusions are present in some Kristallbrocken (Fig. 5a). These are interpreted to be healed microcracks (Supplement 1). All Kristallbrocken contain dispersed inclusions of anhydrite and/or polyhalite and/or brine (Fig. 5a-f, Fig. 6), very similar to those observed and discussed by (Küster et al., 2011).

The fine-grained matrix halite has a grain size of approximately 1 mm (Fig. 7). Halite grains are mostly elongated (KS-06, Kbx1, BS-B, Fig. 3). The fine-grained matrix halite grains commonly have white cores and blue rims (BS-A, KS-13A, KS-05, kbx2, Fig. 3, Fig. 4b, d, Fig. 5g). An interesting observation is that in some of these grains (Fig. 5g), which are elongated,





the white core has the blue overgrowth only in the direction of elongation (eg. pg. 36 in Supplement 1). Very fine-grained matrix halite grains are equiaxed with similar white core and blue mantle as the fine-grained matrix halite, and are associated to high fraction of impurities which have grain sizes of approximately 0.2 mm (KS-13A and B, Fig. 4b)

While in the Barradeel samples the boundary between the Kristalllagen and the fine-grained halite is sharp, in the domal salt this boundary is less sharp, and the fine grains (without subgrains) are locally also present in the Kristallbrocken around their edges. (KS-02, KS-11, KS-08, Fig. 3). These are interpreted to have formed by fluid-assisted grain boundary migration recrystallization, following the interpretation of (Küster et al., 2008, 2011). The recrystallizing halite grains are free of fluid inclusions, with occasional second phase inclusions at grain boundaries (BS-A, KS-13A, KS-13B, KS-05 and KS-02, Fig. 4b, d, Fig. 5b, e, f). The grain boundaries in halite in all samples are rich in fluid inclusions and occasional second phase inclusions. In contrast to the observations of (Küster et al., 2008), subgrains are infrequent in fine-grained salt in the samples studied, making up less than 1 % of total matrix halite volume. When possible, subgrains were digitized (Fig. 3, Supplement1) and piezometry results are presented in Table 1.

Thin anhydrite layers, when enclosed in fine-grained or very fine-grained matrix halite, are strongly deformed by folding and boudinage, together with the enclosing fine-grained or very fine-grained matrix halite. The concentric folding in sample KS-13A (Fig. 4b) indicates that the viscosity of the Anhydrite is much higher than that of the surrounding halite (Adamuszek et al., 2011, 2021). These structures indicate that the matrix Halite was much stronger deformed than the Kristallbrocken. Anhydrite layers directly adjacent to Kristallbrocken are much less deformed but are ruptured together with the Kristallbrocken to form coherent boudins.

EBSD data from sample BS-A are presented in Figure 8. Figure 8a shows Inverse Pole Figure Maps for the points indexed as halite with respect to the horizontal direction and the direction perpendicular to the image plane, respectively. The large Kristallbrocken grains are labelled with 1-5. The two parts of the halite boudin show different crystallographic orientation with a deviation of approximately 60° in the horizontal plane (Supplements 3). Further each Kristallbrocken (1-5) has different crystallographic orientation (Fig. 8a). Figure 8b shows pole figures of the matrix halite after excluding these 5 Kristallbrocken grains from the calculation. The small orientation distribution densities (< 1.8 times random) show that the fine-grained matrix halite has no significant crystallographic preferred orientation (CPO), especially considering the fact that with approximately 1400 grains covered, the statistical base for calculation is comparatively small. Figure 8c shows a Kernel Average Map calculated over a distance of 40µm (second neighbor) with a threshold of 3° in order to enhance the small angle subgrain boundaries. Overlaid in white are low- and high-angle grain boundaries with misorientation of more than 5°. It can be seen that the matrix halite is more or less subgrain-free with very few exceptions in large matrix halite grains, whereas subgrains are present in Kristallbrocken 1 and 5, and in boudin necks of Kristallbrocken 3 and 4. Figure 8d shows the cumulative reference orientation deviation over the areas of Kristallbrocken 3 and 4, based on the higher resolved EBSD measurements of the central Kristallbrockensalz region. The corresponding reference points are marked with white crosses for each of the two grains. Color jumps at the boundary of the individual measurement areas appear due to the movement of the specimen and subsequent recalibration between the individual measurements and should be neglected.



## 290 4 Discussion

Our observations of the Kristallbrockensalz samples correspond closely with those of earlier studies, the most extensive of which is the work of (Küster, 2011) on samples from the same stratigraphic unit, but several hundred km further towards the basin interior. The key shared observations of both studies are: internally deformed megacrystals with solid (polyhalite and anhydrite) and fluid inclusions, subgrains between 0.05 and 0.5 mm, and ruptured in extension to form boudins with dissolution-precipitation in the boudin necks. These megacrystals are surrounded by finer grained halite, with a grain size around 1 mm, with some grains containing subgrains and others being subgrain-free. Solid solution content of Bromide of Kristallbrocken and matrix can be similar or quite different, despite showing the same microstructure. Grain boundaries contain fluid inclusion arrays, and the matrix contains boudinaged and strongly folded thin anhydrite layers indicating high strain in the matrix. Following the interpretation of Löffler (1962) we interpret rupturing of boudins to be tectonic and in favor of other hypothesis (Pape et al., 2002; Richter-Bernburg, 1953) that rupturing of halite crystal layers is diagenetic from subaquatic geysering: although we cannot completely exclude fractures during diagenesis, the presence of abundant subgrains in Kristallbrocken require differential stresses that cannot be generated close to the surface, and this deformation is consistent with formation of boudins.

The interpretation of these observations by Küster et al. (2008, 2011) was that Kristallbrockensalz resemble porphyroclasts in gneissic or mylonitic rocks with a strong rheology contrast between Kristallbrocken and matrix. Kristallbrocken formed from Kristalllagen (of diagenetic origin) by plastic deformation with active [110] slip accompanied by subgrain formation, and by rupturing in extension, while the matrix salt was weaker and more strongly deformed than the Kristallbrocken and deformed by dislocation creep and dynamic recrystallization. We measured subgrain size in the studied micrographs and found average subgrain sizes of 188  $\mu\text{m}$  ( $n=68$ ) in Kristallbrocken (Fig.2.10 in Küster, 2011) and 234  $\mu\text{m}$  ( $n=27$ ) in matrix halite (Fig. 7f in Küster et al., 2008), both from Teutschenthal, that indicate similar differential stresses to values found in our samples (Table 1). The same studies also suggest that matrix halite was secondary, replacing Kristallbrocken by recrystallization. The inferred strong rheology contrast was suggested to be related to ‘monocrystallinity’ (large grain size) and the abundant inclusions in Kristallbrocken by restricting dislocation mobility (Küster et al., 2008).

Our observations have added to the data of Küster et al. (2008, 2011), by providing high resolution microstructures of Gamma-irradiated samples, and crystallographic orientation data by EBSD. In reflected light micrograph we measured subgrain and grain size distributions. measured grain sizes were comparable, but slightly smaller than grain sizes measured on similar samples from the KEM-17 report and stresses from piezometry between 0.8 MPa and 1.5 MPa (Urai et al., 2019) also fit to our observations. We have also shown that subgrains in fine-grained halite are slightly smaller than subgrains in the associated Kristallbrocken.

Based on results of both studies we also conclude that Kristallbrocken deformed by dislocation creep and that there is a large rheology contrast between Kristallbrocken and matrix, a widely occurring phenomenon in the Zechstein basin. However, our results of the Barradeel samples (which we interpret as an undeformed equivalent of the diapiric salt samples) clearly show



that much of the fine- and very fine-grained halite was already present before the onset of salt tectonic deformation, and not only formed by recrystallization of the Kristallbrocken. Because Küster et al. (2008, 2011) did not investigate undeformed equivalents, she did not have access to this information.

The original hypothesis by Küster et al. (2008, 2011) implies that the matrix salt is dynamically recrystallized equivalent of the Kristallbrocken, and deforms by equal contributions of dislocation creep and pressure solution creep (De Bresser et al., 1998; de Bresser et al., 2001; Ter Heege et al., 2005a, b). If this is the case, the predicted weakening would be relatively small (a factor of 2 in strain rate at the same differential stress) and could not explain the large differences in strain between Kristallbrocken and matrix. This effect could be enhanced by the presence of solid inclusions in the Kristallbrocken as proposed by Küster et al. (2008, 2011), however this would lead to larger density of dislocation around the inclusions with corresponding darker color after Gamma-irradiation (Garcia Celma et al., 1988) which was not observed. Finally, solid solution impurities could make the Kristallbrocken more competent (Heard and Ryerson, 1986). The most common solid solution impurity in halite is Bromide (Küster, 2011) but the Kristallbrocken in that study have a comparable structure in samples where Bromide concentration in Kristallbrocken is the same as in the matrix, and in samples where the Bromide concentrations are different, again not supporting this hypothesis.

However, we note that a more extensive analysis of solid solution impurity in these samples would help to further test this hypothesis. Another effect that may make the Kristallbrocken stronger is the presence of adjacent thin anhydrite layers which can form a stronger sandwich - however microstructures with or without sandwiched Anhydrite layers are very similar so this effect cannot be major either (samples BS-A, KS-13A in Fig. 3.)

Here we present an alternative hypothesis to explain the rheology contrast: we propose that the matrix deformed by dominant pressure solution creep while the Kristallbrocken deformed by dislocation creep. Because pressure solution creep is strongly grain size-dependent (see eq. 2), this difference is caused by the large difference in grain size between Kristallbrocken and matrix. Evidence for dominant pressure solution creep in the fine-grained and very fine-grained matrix is provided by the oriented overgrowth structures (Poirier, 1985) (Fig. 5g), the epitaxial overgrowths in boudin necks (Fig. 4d) and the absence of crystallographic preferred orientation as shown by EBSD (Fig. 8). Examples of rock salt microstructures indicating pressure solution creep were presented by (Desbois et al., 2010; Závada et al., 2012), our microstructures are very similar to these. The presence of abundant fluid inclusions on grain boundaries and the evidence for fluid-assisted grain boundary migration recrystallization in both studies show that the required fluid is widely available in this stratigraphic unit.

To quantify the stress-strain conditions corresponding to this hypothesis, in Figure 9 we plotted the data from this study in a differential stress vs strain rate diagram, for a reference temperature of 60 °C. For dislocation creep, we used the BGR-recommended values (Liu, W. et al., 2017; Eickemeier et al., 2021; Popp, 2022) for Kristallbrockensalz, together with a small selection of characteristic values for rock salts from the *Kriechklassen* (German: 'Kriechklasse' = 'creep classes'), and plotted our samples for the values of differential stress obtained from subgrain size piezometry, using the grain sizes of Kristallbrocken and matrix to estimate the expected strain rates. It can be seen that the corresponding strain rates differ by four orders of magnitude, in agreement with the inferred large differences in strain between Kristallbrocken and matrix.



The dynamic recrystallization of Kristallbrocken is also recognized in our samples (Fig. 4b, d, Fig. 5b, e, f), with a very interesting change of the solid inclusions in the Kristallbrocken - these are completely reworked and present in the same configuration in the new grains. However, in our interpretation the fraction of newly recrystallized grains in the matrix is relatively minor. Recrystallization reduces the grain size of large Kristallbrocken single crystals and increases the relative content of finer grained salt. Overgrowth of large Kristallbrocken crystals (increasing their size) has been observed in boudin necks. Hopper crystals indicating primary grains (Pape et al., 2002) were preserved in some BAS samples, but not found in highly deformed domal salt.

The relatively minor newly recrystallized fraction in the strongly deformed diapiric salt samples is interesting, and suggests that grain boundary mobility in nature is lower than in the models of (Peach et al., 2001; Schlöder and Urai, 2005) and that recrystallization and grain growth in salt is more sluggish. Our data do not provide sufficient information to investigate this quantitatively, but we suggest that further work along these lines is interesting.

It is interesting to speculate on the deformation of initial layered salt with the very long Kristalllagen. In simple shear, this rock must have had an extremely anisotropic rheology due to the weak fine-grained and very fine-grained salt. However, in coaxial deformation the Kristalllagen could have carried most of the stress in the salt rock and deformed accordingly by dislocation creep (Bons and Urai, 1994). Once the Kristalllagen were sufficiently fragmented, the rheology of the Kristallbrockensalz becomes a mixture rheology (Bons and Urai, 1994), such that when the Kristallbrocken can form a load-bearing framework, the rock salt deforms by power law creep dominated by dislocation creep in the Kristallbrocken, but when there is sufficient matrix present, the rock salt deforms by Newtonian viscous creep dominated by pressure solution (Jessell et al., 2009). Based on subgrain size analysis we inferred similar differential paleostresses in Kristallbrocken and matrix halite (Fig. 10, even though we had limited number of measurements in matrix halite) which suggest that in our samples the second model was dominant.

In current constitutive models of salt engineering (Albrecht et al., 1993; Hunsche et al., 2003; Bräuer et al., 2011; Kukla et al., 2011; Liu, W. et al., 2017; Popp, 2022) it was long recognized that the creep strain rate of rock salt (as measured at relatively high differential stress) can show several orders of magnitude differences, at the same differential stress and temperature. Based on an extensive dataset, such observations provided the basis for the definition of Kriechklassen which were used to model the evolution of engineered structures (Liu, W. et al., 2017) and are still used to describe a non-Newtonian rheology in salt tectonics numerical modeling (Granado et al., 2021). However, as has been reviewed above, extrapolation of these data to low differential stress predicts orders of magnitude lower creep rates than measured in experiments (Brouard and Bérest, 1998; Bérest et al., 2019) and predicted by microphysical models of pressure solution creep (Spiers et al., 1986; Urai et al., 1986b; Spiers et al., 1990). Integration of these mechanisms into engineering constitutive equations is sometimes conducted (e.g. Zill et al., 2022; Buijze et al., 2022). However, it requires data on the grain size of the rock salt to be modeled, together with microstructural characterization, and we recommend to include grain sizes in engineering prediction and create pressure solution-creep classes.



## 390 5 Conclusion

In this study, we present examples of flat-lying and diapiric Zechstein salt from the same formation (Z2), which was naturally deformed under low differential stresses between 1 and 2 MPa, providing a natural laboratory to study salt rheology under conditions which are difficult to study in the laboratory but relevant for predicting the evolution of engineered structures over long time scales. The gneissic Kristallbrocken salt deforms by dislocation creep and pressure solution processes depending on the grain size. The fine-grained matrix halite is weaker and deforms with a higher strain rate by pressure solution and dynamic recrystallization while the Kristallbrocken mega grains tectonically boudinage and deform by dislocation creep. We infer that this large rheology contrasts in halite deformation at low differential stresses is caused by grain size-dependent dissolution-precipitation creep.

At present, grain size measurements are not available for most of the Zechstein salts used in salt engineering, and we recommend the creation of a salt microstructure knowledge base which will help predicting creep rates at low differential stress.

Further studies to better define solid solution impurity contents, the role of mineral impurities and the contribution of dynamic recrystallization with grain boundary migration to solution precipitation processes will help to test the operating deformation mechanisms in more detail.

## 405 Supplements

1. Additional Micrographs
2. High resolution sample overview scans, piezometry images and results
3. EBSD material
4. BIB-SEM material
- 410 5. XRD analysis results

## Data availability statement

The supplementary material has been uploaded to Zenodo repository and is available at <https://doi.org/10.5281/zenodo.6839080>

## Author contribution

415 JB carried out the study and designed figures. JLU and JS designed the study. JK and JLU selected samples. AS did EBSD measurements and Fig. 8. JB and JLU prepared the manuscript with contributions from all co-authors, which were also involved in scientific discussions.



## Competing interests

The authors declare that they have no conflict of interest.

## 420 Acknowledgements

We would like to acknowledge support of Nedmag Industries and RWTH Aachen University funding for completion of this study. Sample preparation of Werner Kraus was much appreciated. We further thank Marc Sadler for use of images in Figure 4c and Figure 5h from his MSc Thesis (Sadler, 2012).

## References

- 425 Adamuszek, M., Schmid, D. W., and Dabrowski, M.: Fold geometry toolbox – Automated determination of fold shape, shortening, and material properties, *J. Struct. Geol.*, 33, 1406–1416, <https://doi.org/10.1016/j.jsg.2011.06.003>, 2011.
- Adamuszek, M., Tămaş, D. M., Barabasch, J., and Urai, J. L.: Rheological stratification in impure rock salt during long-term creep: morphology, microstructure, and numerical models of multilayer folds in the Ocnele Mari salt mine, Romania, *Solid Earth*, 12, 2041–2065, <https://doi.org/10.5194/se-12-2041-2021>, 2021.
- 430 Albrecht, H., Hunsche, U. E., and Schulze, O.: Results from the application of the laboratory test program for mapping homogeneous parts in the Gorleben salt dome, 10th national rock mechanics symposium, Essen, Germany, 155–158, 1993.
- Kaart boringen | NLOG: <https://www.nlog.nl/kaart-boringen>, last access: 15 February 2022.
- Barabasch, J., Urai, J. L., Raith, A. F., and de Jager, J.: The early life of a salt giant: 3D seismic study on syntectonic Zechstein salt and stringer deposition on the Friesland Platform, Netherlands, *Z. Dtsch. Geol. Ges.*, 170, 273–288, 435 <https://doi.org/10.1127/zdgg/2019/0186>, 2019.
- Baumann, T. S., Kaus, B. J. P., and Popov, A. A.: Deformation and stresses related to the Gorleben salt structure: Insights from 3D numerical models, in: *Mechanical behavior of salt IX*, edited by: Fahland, S., Hammer, J., Hansen, F., Heusermann, S., Lux, K.-H., and Minkley, W., BGR, Hannover, Germany, 597–609, 2018.
- Bérest, P., Béraud, J. F., Brouard, B., Blum, P. A., Charpentier, J. P., de Greef, V., Gharbi, H., and Valès, F.: Very slow creep tests on salt samples, *EPJ Web of Conferences*, 6, 22002, <https://doi.org/10.1051/epjconf/20100622002>, 2010.
- 440 Bérest, P., Gharbi, H., Brouard, B., Brückner, D., DeVries, K., Hévin, G., Hofer, G., Spiers, C., and Urai, J. L.: Very Slow Creep Tests on Salt Samples, *Rock. Mech. Rock. Eng.*, 52, 2917–2934, <https://doi.org/10.1007/s00603-019-01778-9>, 2019.
- Bons, P. D. and Urai, J. L.: Experimental deformation of two-phase rock analogues, *Mater. Sci. Eng.*, 175, 221–229, [https://doi.org/10.1016/0921-5093\(94\)91061-8](https://doi.org/10.1016/0921-5093(94)91061-8), 1994.
- 445 Bräuer, V., Eickenmeier, R., Eisenburger, D., Grisseemann, C., Hesser, J., Heusermann, S., Kaiser, D., Nipp, H.-K., Nowak, T., Plischke, I., Schnier, H., Schulze, O., Sönnke, J., and Weber, J. R.: Description of the Gorleben site part 4: Geotechnical exploration of the Gorleben salt dome, BGR, Hannover, Germany, 2011.



- de Bresser, J. H. P., Ter Heege, J. H., and Spiers, C. J.: Grain size reduction by dynamic recrystallization: can it result in major rheological weakening?, *Int. J. Earth Sciences (Geol. Rundsch.)*, 90, 28–45, <https://doi.org/10.1007/s005310000149>, 2001.
- Brouard, B. and Bérest, P.: A tentative classification of salts according to their creep properties, SMRI Spring 1998 Meeting, 19–22 April 1998, New Orleans, Louisiana, USA, 18–38, 1998.
- Brouard, B., Bérest, P., Héas, J.-Y., Fourmaintraux, D., de Laguérie, P., and You, T.: An in situ creep test in advance of abandoning a salt cavern, SMRI Fall 2004 Technical Meeting, 3–5 October 2004, Berlin, Germany, 45–69, 2004.
- 455 Buijze, L., Heege, J. T., and Wassing, B.: Finite Element modeling of natural sealing of wellbores in salt using advanced, laboratory-based salt creep laws, in: *The Mechanical Behavior of Salt X*, CRC Press, 2022.
- Carter, N. L. and Hansen, F. D.: Creep of rocksalt, *Tectonophysics*, 92, 275–333, [https://doi.org/10.1016/0040-1951\(83\)90200-7](https://doi.org/10.1016/0040-1951(83)90200-7), 1983.
- 460 Carter, N. L., Hansen, F. D., and Senseny, P. E.: Stress magnitudes in natural rock salt, *J. Geophys. Res.*, 87, 9289, <https://doi.org/10.1029/JB087iB11p09289>, 1982.
- Carter, N. L., Horseman, S. T., Russell, J. E., and Handin, J.: Rheology of rocksalt, *J. Struct. Geol.*, 15, 1257–1271, [https://doi.org/10.1016/0191-8141\(93\)90168-A](https://doi.org/10.1016/0191-8141(93)90168-A), 1993.
- Chemia, Z., Schmeling, H., and Koyi, H.: The effect of the salt viscosity on future evolution of the Gorleben salt diapir, Germany, *Tectonophysics*, 473, 446–456, <https://doi.org/10.1016/j.tecto.2009.03.027>, 2009.
- 465 De Bresser, J. H. P., Peach, C. J., Reijs, J. P. J., and Spiers, C. J.: On dynamic recrystallization during solid state flow: Effects of stress and temperature, *Geophys. Res. Lett.*, 25, 3457–3460, <https://doi.org/10.1029/98GL02690>, 1998.
- Desbois, G., Závada, P., Schléder, Z., and Urai, J. L.: Deformation and recrystallization mechanisms in actively extruding salt fountain: Microstructural evidence for a switch in deformation mechanisms with increased availability of meteoric water and decreased grain size (Qum Kuh, central Iran), *J. Struct. Geol.*, 32, 580–594, <https://doi.org/10.1016/j.jsg.2010.03.005>, 2010.
- 470 Desbois, G., Urai, J. L., Schmatz, J., Závada, P., and de Bresser, J. H. P.: The distribution of fluids in natural rock salt to understand deformation mechanism, in: *Mechanical behaviour of Salt VII*, edited by: Bérest, P., Ghoreychi, M., Hadj-Hassen, F., and Tijani, M., Taylor & Francis Group, London, United Kingdom, 3–12, 2012.
- Dooley, T. P., Jackson, M. P. A., Jackson, C. A.-L., Hudec, M. R., and Rodriguez, C. R.: Enigmatic structures within salt walls of the Santos Basin—Part 2: Mechanical explanation from physical modelling, *J. Struct. Geol.*, 75, 163–187, <https://doi.org/10.1016/j.jsg.2015.01.009>, 2015.
- 475 Drury, M. R. and Urai, J. L.: Deformation-related recrystallization processes, *Tectonophysics*, 172, 235–253, [https://doi.org/10.1016/0040-1951\(90\)90033-5](https://doi.org/10.1016/0040-1951(90)90033-5), 1990.
- Eickemeier, R., Beese, S., Maniatis, G., and Fahland, S.: Sensitivitätsstudien zur gebirgsmechanischen Beurteilung der Integrität der Salzstockbarriere im Südfeld Bartensleben – Teil 5, BGR, Hannover, Germany, 2021.
- 480 Fiduk, J. C. and Rowan, M. G.: Analysis of folding and deformation within layered evaporites in Blocks BM-S-8 & -9, Santos Basin, Brazil, in: *Salt tectonics, sediments and prospectivity*, edited by: Alsop, G. I., Archer, S. G., Hartley, A. J.,





- Grant, N. T., and Hodgkinson, R., The Geological Society, London, United Kingdom, 471–487, <https://doi.org/10.1144/SP363.22>, 2012.
- 485 Garcia Celma, A., Urai, J. L., and Spiers, C. J.: A laboratory investigation into the interaction of recrystallization and radiation damage effects in polycrystalline salt rocks, Office for Official Publications of the European Communities, Luxembourg, 125 pp., 1988.
- Geluk, M. C.: Late Permian (Zechstein) carbonate-facies maps, the Netherlands, *Geol Mijnbouw*, 79, 17–27, <https://doi.org/10.1017/S0016774600021545>, 2000.
- 490 Geluk, M. C., Paar, W. A., and Fokker, P. A.: Salt, in: *Geology of the Netherlands*, edited by: Wong, T. E., Batjes, D. A. J., and de Jager, J., Royal Netherlands Academy of Arts and Sciences, Amsterdam, Netherlands, 283–294, 2007.
- van Gent, H. W., Urai, J. L., and de Keijzer, M.: The internal geometry of salt structures – A first look using 3D seismic data from the Zechstein of the Netherlands, *J. Struct. Geol.*, 33, 292–311, <https://doi.org/10.1016/j.jsg.2010.07.005>, 2011.
- Granado, P., Ruh, J. B., Santolaria, P., Strauss, P., and Muñoz, J. A.: Stretching and Contraction of Extensional Basins With Pre-Rift Salt: A Numerical Modeling Approach, *Frontiers in Earth Science*, 9, 2021.
- 495 Hampel, A.: *Verbundprojekt: Vergleich aktueller Stoffgesetze und Vorgehensweisen anhand von Modellberechnungen zum thermo-mechanischen Verhalten und zur Verheilung von Steinsalz – Ergebnisbericht zum Teilvorhaben 1*, Projektträger Karlsruhe, Wassertechnologie und Entsorgung (PTKA-WTE), Karlsruher Institut für Technologie (KIT), Mainz, Germany, 2016.
- 500 Hampel, A., Schulze, O., Heemann, U., Zetsche, F., Günther, R.-M., Salzer, K., Minkley, W., Hou, M. Z., Wolters, R., Düsterloh, U., Zapf, D., Rokahr, R. B., and Pudewills, A.: BMBF-Verbundvorhaben: Die Modellierung des mechanischen Verhaltens von Steinsalz: Vergleich aktueller Stoffgesetze und Vorgehensweisen. Synthesebericht, Projektträger Forschungszentrum Karlsruhe (PTKA), Bereich Wassertechnologie und Entsorgung (WTE), Karlsruhe, Germany, 2007.
- 505 Heard, H. C. and Ryerson, F. J.: Effect of cation impurities on steady-state flow of salt, in: *Mineral and rock deformation: Laboratory studies*, edited by: Hobbs, B. E. and Heard, H. C., American Geophysical Union, Washington, D.C., USA, 99–115, <https://doi.org/10.1029/GM036p0099>, 1986.
- Hudleston, P. J. and Treagus, S. H.: Information from folds: A review, *J. Struct. Geol.*, 32, 2042–2071, <https://doi.org/10.1016/j.jsg.2010.08.011>, 2010.
- 510 Hunsche, U. and Hampel, A.: Rock salt — the mechanical properties of the host rock material for a radioactive waste repository, *Eng. Geol.*, 52, 271–291, [https://doi.org/10.1016/S0013-7952\(99\)00011-3](https://doi.org/10.1016/S0013-7952(99)00011-3), 1999.
- Hunsche, U., Schulze, O., Walter, F., and Plischke, I.: *Thermomechanisches Verhalten von Salzgestein*, BGR, Hannover, Germany, 2003.
- Jackson, M. P. A. and Hudec, M. R.: *Salt Tectonics: Principles and Practice*, Cambridge University Press, <https://doi.org/10.1017/9781139003988>, 2017.
- 515 Jackson, M. P. A., Vendeville, B. C., and Schultz-Ela, D. D.: Structural dynamics of salt systems, *Annu. Rev. Earth Planet. Sci.*, 22, 93–117, <https://doi.org/10.1146/annurev.ea.22.050194.000521>, 1994.
- Jessell, M. W., Bons, P. D., Griera, A., Evans, L. A., and Wilson, C. J. L.: A tale of two viscosities, *J. Struct. Geol.*, 31, 719–736, <https://doi.org/10.1016/j.jsg.2009.04.010>, 2009.



- 520 Juez-Larré, J., van Gessel, S., Dalman, R., Remmelts, G., and Groenenberg, R.: Assessment of underground energy storage potential to support the energy transition in the Netherlands, *First Break*, 37, 57–66, <https://doi.org/10.3997/1365-2397.n0039>, 2019.
- van Keken, P. E., Spiers, C. J., van den Berg, A. P., and Muzyert, E. J.: The effective viscosity of rocksalt: Implementation of steady-state creep laws in numerical models of salt diapirism, *Tectonophysics*, 225, 457–476, [https://doi.org/10.1016/0040-1951\(93\)90310-G](https://doi.org/10.1016/0040-1951(93)90310-G), 1993.
- 525 Komoróczy, A., Abe, S., and Urai, J. L.: Meshless numerical modeling of brittle–viscous deformation: first results on boudinage and hydrofracturing using a coupling of discrete element method (DEM) and smoothed particle hydrodynamics (SPH), *Comput. Geosci.*, 17, 373–390, <https://doi.org/10.1007/s10596-012-9335-x>, 2013.
- Kukla, P. A., Pechinig, R., and Urai, J. L.: Sichtung und Bewertung der Standortdaten Gorleben: Bericht zum Arbeitspaket 2: Vorläufige Sicherheitsanalyse für den Standort Gorleben, Gesellschaft für Anlagen- und Reaktorsicherheit (GRS) mbH, 530 Cologne, Germany, 2011.
- Kukla, P. A., Urai, J. L., Raith, A., Li, S., Barabasch, J., and Strozyk, F.: The European Zechstein Salt Giant—Trusheim and Beyond, 37th Annual GCSSEPM Foundation Perkins-Rosen Research Conference., 2019.
- Küster, Y.: Bromide characteristics and deformation mechanisms of naturally deformed rock salt of the German Zechstein Basin, Georg-August-Universität, Göttingen, Germany, 221 pp., 2011.
- 535 Küster, Y., Leiss, B., and Schramm, M.: Structural characteristics of the halite fabric type ‘Kristallbrocken’ from the Zechstein Basin with regard to its development, *Int. J. Earth Sci.*, 99, 505–526, <https://doi.org/10.1007/s00531-008-0399-8>, 2008.
- Küster, Y., Schramm, M., Bornemann, O., and Leiss, B.: Bromide distribution characteristics of different Zechstein 2 rock salt sequences of the Southern Permian Basin: a comparison between bedded and domal salts, *Sedimentology*, 56, 1368–540 1391, <https://doi.org/10.1111/j.1365-3091.2008.01038.x>, 2009.
- Küster, Y., Schramm, M., and Leiss, B.: Compositional and microstructural characterisation of solid inclusions in the laminated halite type “Kristallbrocken” with regard to its formation in the Central European Zechstein Basin, *Z. Dt. Ges. Geowiss.*, 162, 277–294, <https://doi.org/10.1127/1860-1804/2011/0162-0277>, 2011.
- Laier, T., Kockel, F., Geluk, M. C., Pokorsky, J., and Lott, G.K.: Section A (Geology), in: *NW European Gas Atlas*, edited by: Lokhorst, A., NITG-TNO, Haarlem, 1998.
- 545 Leitner, C., Neubauer, F., Urai, J. L., and Schoenherr, J.: Structure and evolution of a rocksalt-mudrock-tectonite: The haselgebirge in the Northern Calcareous Alps, *J. Struct. Geol.*, 33, 970–984, <https://doi.org/10.1016/j.jsg.2011.02.008>, 2011.
- Liu, W., Völkner, E., Minkley, W., and Popp, T.: Zusammenstellung der Materialparameter für THM-Modellberechnungen: Ergebnisse aus dem Vorhaben KOSINA, BGR, Hannover, Germany, 2017.
- 550 Löffler, J.: Zur Genese der Augensalze im Zechstein der Deutschen Demokratischen Republik, *Z. angew. Geol.*, 11, 583–589, <https://doi.org/10.1515/9783112558201-006>, 1962.
- Lopez-Sanchez, M. A. and Llana-Fúnez, S.: An evaluation of different measures of dynamically recrystallized grain size for paleopiezometry or paleowattometry studies, *Solid Earth*, 6, 475–495, <https://doi.org/10.5194/se-6-475-2015>, 2015.



- Means, W. D. and Ree, J. H.: Seven types of subgrain boundaries in octachloropropane, *J. Struct. Geol.*, 10, 765–770, [https://doi.org/10.1016/0191-8141\(88\)90083-1](https://doi.org/10.1016/0191-8141(88)90083-1), 1988.
- van Noort, R., Visser, H. J. M., and Spiers, C. J.: Influence of grain boundary structure on dissolution controlled pressure solution and retarding effects of grain boundary healing, *J. Geophys. Res.*, 113, B03201, <https://doi.org/10.1029/2007JB005223>, 2008.
- Pape, T., Michalzik, D., and Bornemann, O.: Chevronkristalle im Kristallbrockensalz (Zechstein 2) des Salzstocks Gorleben - Primärgefüge salinarer Flachwassersedimentation im Zechsteinbecken, *Z. Dt. Ges. Geowiss.*, 115–129, <https://doi.org/10.1127/zdgg/153/2002/115>, 2002.
- Peach, C. J., Spiers, C. J., and Trimby, P. W.: Effect of confining pressure on dilatation, recrystallization, and flow of rock salt at 150°C, *J. Geophys. Res.*, 106, 13315–13328, <https://doi.org/10.1029/2000JB900300>, 2001.
- Peel, F. J.: The engines of gravity-driven movement on passive margins: Quantifying the relative contribution of spreading vs. gravity sliding mechanisms, *Tectonophysics*, 633, 126–142, <https://doi.org/10.1016/j.tecto.2014.06.023>, 2014.
- Poirier, J.-P.: *Creep of Crystals: High-Temperature Deformation Processes in Metals, Ceramics and Minerals*, 1st ed., Cambridge University Press, <https://doi.org/10.1017/CBO9780511564451>, 1985.
- Popp, T.: *Eigenschaften und Potential stratiformer Salz-Formationen für die Endlagerung hochradioaktiver Abfälle*, Institut für Gebirgsmechanik IfG, Leipzig, Germany, 2022.
- Popp, T. and Hansen, F. D.: Creep at low deviatoric stress, in: *Proceedings of the 8th US/German workshop on salt repository research, design, and operation*, edited by: Hansen, F. D., Steininger, W., Bollingerfehr, W., Kuhlman, K., and Dunagan, S., Sandia National Laboratories, Albuquerque, New Mexico, USA, 21–24, 2018.
- Richter-Bernburg, G.: Über salinare Sedimentation, *Z. Dt. Ges. Geowiss.*, 105, 593–645, 1953.
- Rowan, M. and Krzywiec, P.: The Szamotuły salt diapir and Mid-Polish Trough: Decoupling during both Triassic-Jurassic rifting and Alpine inversion, *Interpretation*, 2, <https://doi.org/10.1190/INT-2014-0028.1>, 2014.
- Rowan, M. G., Urai, J. L., Fiduk, J. C., and Kukla, P. A.: Deformation of intrasalt competent layers in different modes of salt tectonics, *Solid Earth*, 10, 987–1013, <https://doi.org/10.5194/se-10-987-2019>, 2019.
- Sadler, M.: *The distribution and morphology of grain boundary fluids in natural rock salt*, M.Sc., RWTH Aachen University, 2012.
- Schenk, O. and Urai, J. L.: Microstructural evolution and grain boundary structure during static recrystallization in synthetic polycrystals of sodium chloride containing saturated brine, *Contrib Mineral Petrol*, 146, 671–682, <https://doi.org/10.1007/s00410-003-0522-6>, 2004.
- Schenk, O., Urai, J. L., and Piazzolo, S.: Structure of grain boundaries in wet, synthetic polycrystalline, statically recrystallizing halite - evidence from cryo-SEM observations, *Geofluids*, 6, 93–104, <https://doi.org/10.1111/j.1468-8123.2006.00134.x>, 2006.
- Schindelin, J., Arganda-Carreras, I., Frise, E., Kaynig, V., Longair, M., Pietzsch, T., Preibisch, S., Rueden, C., Saalfeld, S., Schmid, B., Tinevez, J.-Y., White, D. J., Hartenstein, V., Eliceiri, K., Tomancak, P., and Cardona, A.: Fiji: an open-source platform for biological-image analysis, *Nat Methods*, 9, 676–682, <https://doi.org/10.1038/nmeth.2019>, 2012.



- 590 Schlöder, Z. and Urai, J. L.: Microstructural evolution of deformation-modified primary halite from the Middle Triassic Röt Formation at Hengelo, The Netherlands, *Int J Earth Sci (Geol Rundsch)*, 94, 941–955, <https://doi.org/10.1007/s00531-005-0503-2>, 2005.
- Schlöder, Z. and Urai, J. L.: Deformation and recrystallization mechanisms in mylonitic shear zones in naturally deformed extrusive Eocene–Oligocene rocksalt from Eyvanekey plateau and Garmsar hills (central Iran), *J. Struct. Geol.*, 29, 241–255, <https://doi.org/10.1016/j.jsg.2006.08.014>, 2007.
- 595 Schmalholz, S. M. and Mancktelow, N.: Folding and necking across the scales: a review of theoretical and experimental results and their applications, *Solid Earth*, <https://doi.org/10.5194/se-2016-80>, 2016.
- Schmalholz, S. M. and Podladchikov, Y. Yu.: Strain and competence contrast estimation from fold shape, *Tectonophysics*, 340, 195–213, [https://doi.org/10.1016/S0040-1951\(01\)00151-2](https://doi.org/10.1016/S0040-1951(01)00151-2), 2001.
- Schmatz, J., Schenk, O., and Urai, J. L.: The interaction of migrating grain boundaries with fluid inclusions in rock analogues: the effect of wetting angle and fluid inclusion velocity, *Contrib Mineral Petrol*, 162, 193–208, <https://doi.org/10.1007/s00410-010-0590-3>, 2011.
- 600 Schultze-Ela, D. D., Jackson, M. P. A., and Vendeville, B. C.: Mechanics of active salt diapirism, *Tectonophysics*, 228, 275–312, [https://doi.org/10.1016/0040-1951\(93\)90345-K](https://doi.org/10.1016/0040-1951(93)90345-K), 1993.
- Seidl, E.: Die permische salzlagerstätte im Graf Moltke schalcht und in der umgebung von Schönebeck a. d. Elbe: Beziehung zwischen mechanismus der gebirgsbildung und innerer umformung der salzlagerstätte, Königlich Preußische Geologische Landesanstalt, Berlin, Germany, 104 pp., 1914.
- 605 Simon, P.: Stratigraphie und Bromgehalt des Staßfurt-Steinsalzes (Zechstein 2) im hannoverschen Kalisalzbergbauegebiet 67–126, *Geol. Jhrbch*, 90, 67–126, 1972.
- Spiers, C. J. and Carter, N. L.: Microphysics of rocksalt flow in nature, in: 4th Conference on the Mechanical Behavior of Salt, edited by: Aubertin, M. and Hardy, Jr., H. R., Trans Tech Publications, Clausthal-Zellerfeld, Germany, 115–128, 1998.
- 610 Spiers, C. J., Urai, J. L., Lister, G. S., Boland, J. N., and Zwart, H. J.: The influence of fluid-rock interaction on the rheology of salt rock, Commission of the European Communities, Luxembourg, 1986.
- Spiers, C. J., Schutjens, P. M. T. M., Brzesowsky, R. H., Peach, C. J., Liezenberg, J. L., and Zwart, H. J.: Experimental determination of constitutive parameters governing creep of rocksalt by pressure solution, in: Deformation mechanisms, rheology and tectonics, edited by: Knipe, R. J. and Rutter, E. H., The Geological Society, London, United Kingdom, 215–227, <https://doi.org/10.1144/GSL.SP.1990.054.01.21>, 1990.
- 615 Strozyk, F., Urai, J. L., van Gent, H., de Keijzer, M., and Kukla, P. A.: Regional variations in the structure of the Permian Zechstein 3 intrasalt stringer in the northern Netherlands: 3D seismic interpretation and implications for salt tectonic evolution, *Interpretation*, 2, SM101–SM117, <https://doi.org/10.1190/INT-2014-0037.1>, 2014.
- 620 Talbot, C. J.: Fold trains in a glacier of salt in southern Iran, *J. Struct. Geol.*, 1, 5–18, [https://doi.org/10.1016/0191-8141\(79\)90017-8](https://doi.org/10.1016/0191-8141(79)90017-8), 1979.
- Talbot, C. J. and Aftabi, P.: Geology and models of salt extrusion at Qum Kuh, central Iran, *J. Geol. Soc.*, London, 161, 321–334, <https://doi.org/10.1144/0016-764903-102>, 2004.



- 625 Tămaş, D. M., Tămaş, A., Barabasch, J., Rowan, M. G., Schléder, Z., Krézsek, C., and Urai, J. L.: Low-Angle Shear Within the Exposed Mânzălești Diapir, Romania: Salt Decapitation in the Eastern Carpathians Fold-and-Thrust Belt, *Tectonics*, 40, e2021TC006850, <https://doi.org/10.1029/2021TC006850>, 2021.
- Ter Heege, J. H., De Bresser, J. H. P., and Spiers, C. J.: Dynamic recrystallization of wet synthetic polycrystalline halite: dependence of grain size distribution on flow stress, temperature and strain, *Tectonophysics*, 396, 35–57, <https://doi.org/10.1016/j.tecto.2004.10.002>, 2005a.
- 630 Ter Heege, J. H., de Bresser, J. H. P., and Spiers, C. J.: Rheological behaviour of synthetic rocksalt: the interplay between water, dynamic recrystallization and deformation mechanisms, *J. Struct. Geol.*, 27, 948–963, <https://doi.org/10.1016/j.jsg.2005.04.008>, 2005b.
- Trusheim, F.: Über Halokinese und ihre Bedeutung für die strukturelle Entwicklung Norddeutschlands, *Z. Dt. Ges. Geowiss.*, 111–158, 1957.
- 635 Urai, J. L. and Spiers, C. J.: The effect of grain boundary water on deformation mechanisms and rheology of rocksalt during long-term deformation, in: *The mechanical behavior of salt – understanding of THMC processes in salt*, edited by: Wallner, M., Lux, K.-H., Minkley, W., and Hardy, Jr., H. R., Taylor & Francis, Hannover, Germany, 149–158, <https://doi.org/10.1201/9781315106502-17>, 2007.
- Urai, J. L., Means, W. D., and Lister, G. S.: Dynamic Recrystallization of Minerals, in: *Mineral and Rock Deformation*, 640 *American Geophysical Union (AGU)*, 161–199, <https://doi.org/10.1029/GM036p0161>, 1986a.
- Urai, J. L., Spiers, C. J., Zwart, H. J., and Lister, G. S.: Weakening of rock salt by water during long-term creep, *Nature*, 324, 554–557, <https://doi.org/10.1038/324554a0>, 1986b.
- Urai, J. L., Spiers, C. J., Peach, C. J., Franssen, R. C. M. W., and Liezenberg, J. L.: Deformation mechanisms operating in naturally deformed halite rocks as deduced from microstructural investigations, *Geol Mijnbouw*, 66, 165–176, 1987.
- 645 Urai, J. L., Schléder, Z., Spiers, C. J., and Kukla, P. A.: Flow and transport properties of salt rocks, in: *Dynamics of complex intracontinental basins: The central European basin system*, edited by: Littke, R., Bayer, U., Gajewski, D., and Nelskamp, S., Springer, Berlin, Germany, 277–290, 2008.
- Urai, J. L., Schmatz, J., and Klaver, J.: Report, Project KEM-17 Over-pressured salt solution mining caverns and leakage mechanisms, Ministry of Economic Affairs and Climate, The Netherlands, 2019.
- 650 Wawersik, W. R. and Zeuch, D. H.: Modeling and mechanistic interpretation of creep of rock salt below 200°C, *Tectonophysics*, 121, 125–152, [https://doi.org/10.1016/0040-1951\(86\)90040-5](https://doi.org/10.1016/0040-1951(86)90040-5), 1986.
- Wenkert, D.: The flow of salt glaciers, *Geophys. Res. Lett.*, 6, 523–26, 1979.
- Závada, P., Desbois, G., Schwedt, A., Lexa, O., and Urai, J. L.: Extreme ductile deformation of fine-grained salt by coupled solution-precipitation creep and microcracking: Microstructural evidence from perennial Zechstein sequence (Neuhof salt 655 mine, Germany), *J. Struct. Geol.*, 37, 89–104, <https://doi.org/10.1016/j.jsg.2012.01.024>, 2012.
- Závada, P., Desbois, G., Urai, J. L., Schulmann, K., Rahmati, M., and Lexa, O.: Impact of solid second phases on deformation mechanisms of naturally deformed salt rocks (Kuh-e-Namak, Dashti, Iran) and rheological stratification of the Hormuz Salt Formation, *J. Struct. Geol.*, 74, 117–144, 2015.



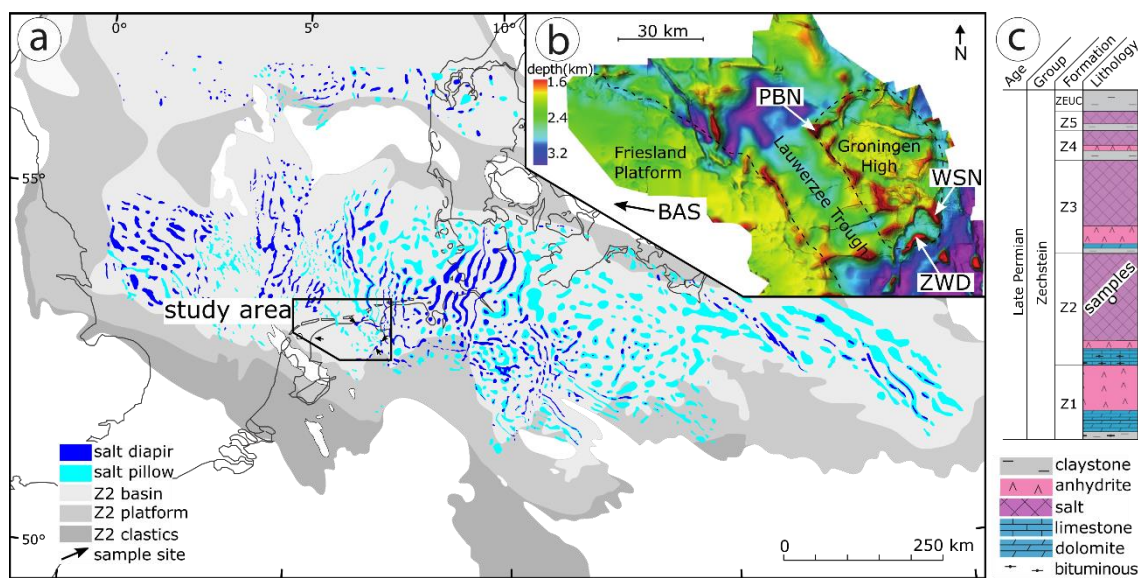


660 Zill, F., Wang, W., and Nagel, T.: Influence of THM process coupling and constitutive models on the simulated evolution of deep salt formations during glaciation, in: *The Mechanical Behavior of Salt X*, edited by: de Bresser, J. H. P., Drury, M. R., Fokker, P. A., Gazzani, M., Hangx, S. J. T., Niemeijer, A. R., and Spiers, C. J., CRC Press, London, 353–362, <https://doi.org/10.1201/9781003295808-33>, 2022.

Zulauf, J., Zulauf, G., Göttlich, J., and Peinl, M.: Formation of chocolate-tablet boudins: Results from scaled analogue models, *J. Struct. Geol.*, 68, 97–111, <https://doi.org/10.1016/j.jsg.2014.09.005>, 2014.

665

Figures



670 **Figure 1:** a) Zechstein salt structures in the Permian basin and Z2 carbonate facies distribution after (Laier, T. et al., 1998; Geluk, 2000). b) Study area (indicated in (a)) after Strozyk et al., (2014) showing top salt depth from seismic interpretation and well locations. BAS=Barradeel, PBN=Pieterburen, WSN=Winschoten and ZWD=Zuidwending. c) Stratigraphy of Zechstein salt in the Netherlands after Geluk et al. (2007) with stratigraphic position of studied samples.

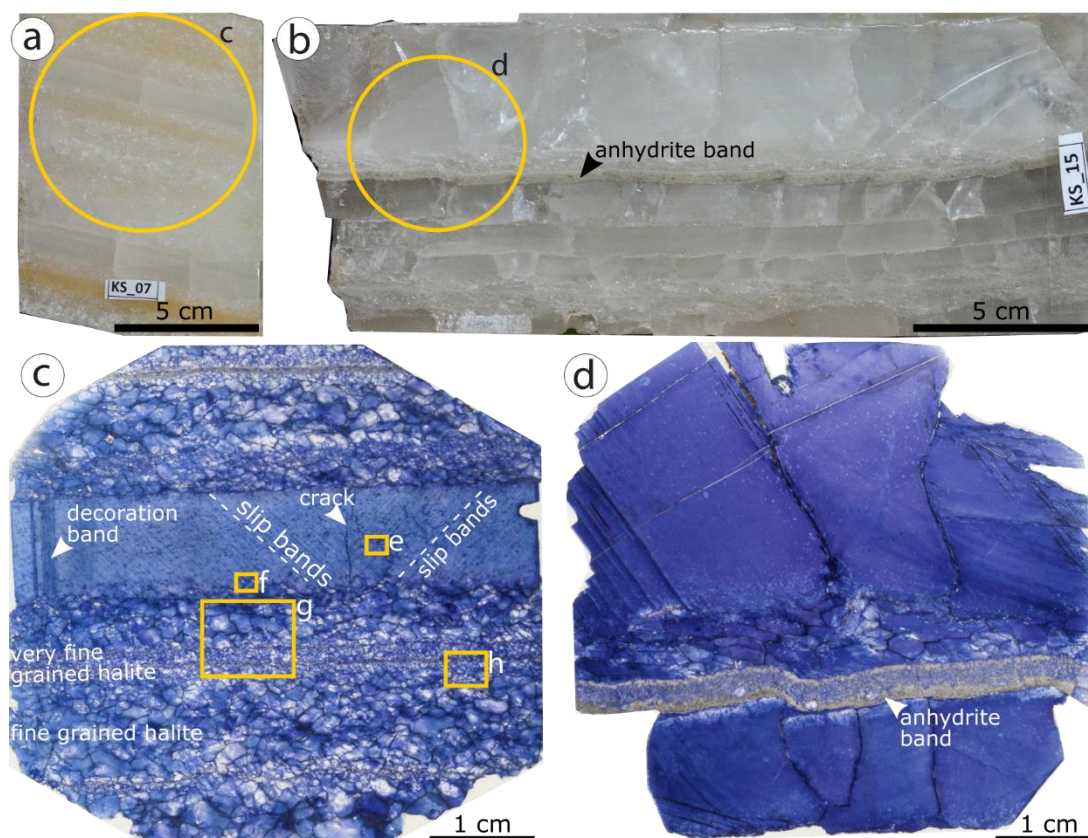


**Figure 2:** a) Reflected light photograph of slabs (KS-07 from Barradeel) used for microstructural analysis showing layered white and honey colored salt with variable grain sizes and milky Kristallagen with internal lamination. b) Slab specimen KS-15 of Barradeel used for microstructural analysis showing layered transparent and white salt with Kristallagen up to 5 cm thicknesses with cracks. Small fold in 5 mm thick anhydrite band is bend following the displaced crystal layer. c) overview of gamma decorated thin section of sample KS-07 in transmitted light (location indicated in a) showing Kristallagen with abundant inclusions and decorated slip bands, dark blue decorated bands parallel to crack and layers of fine and very fine-grained halite with white cores and blue rims. d) overview of gamma decorated thin section of sample KS-15 in transmitted light (location indicated in b)) showing inclusion poor crystal layers that are slightly displaced and layers of fine-grained halite, with some grains showing a white overgrowth. Anhydrite-halite band is slightly bent and contains abundant halite mineral inclusions of up to 2mm.



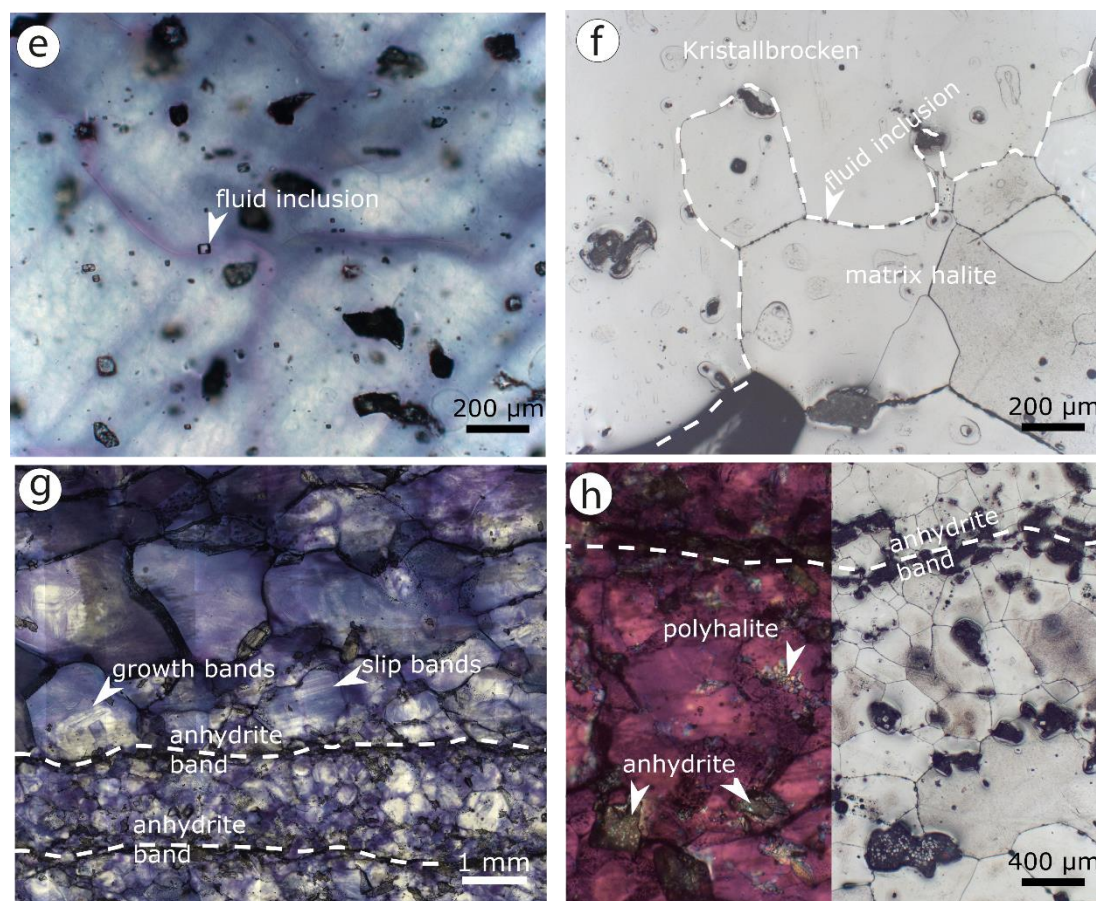
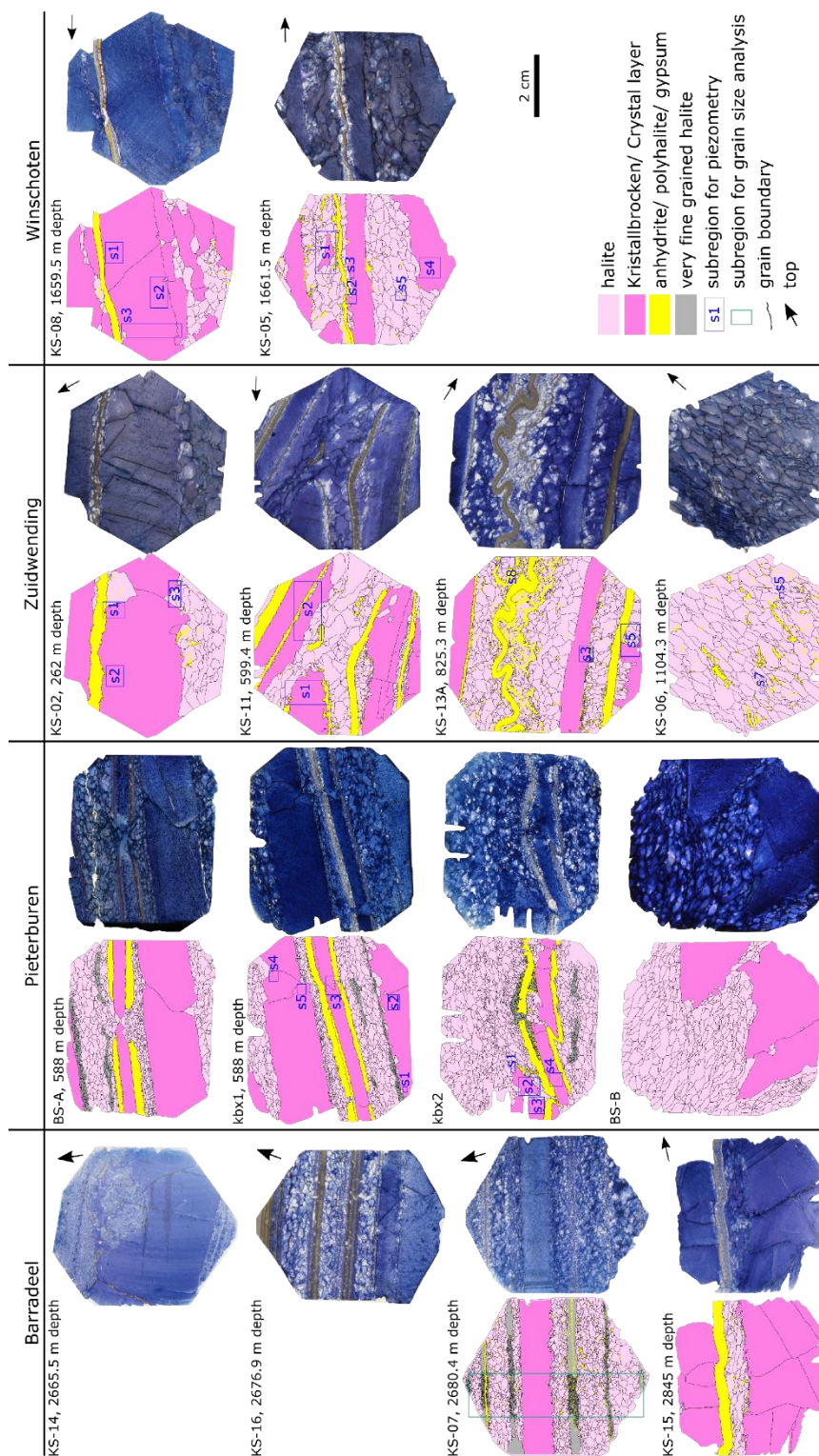


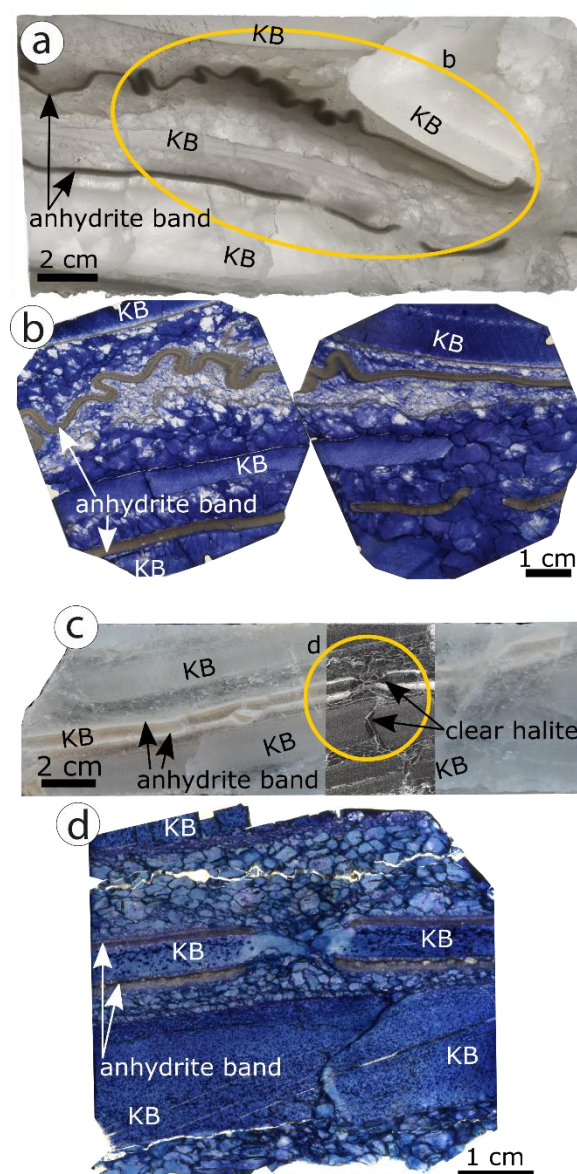
**Figure 2:** e) Micrograph (location indicated in (Fig. 2c)) showing gamma decorated slip bands and cellular blue structures at two different scales, abundant solid inclusions up to 200  $\mu\text{m}$  and fluid inclusions with gas bubbles. f) Reflected light image of Kristallbrocken and fine-grained halite with fluid inclusions and anhydrite at grain boundaries. g) transmitted light micrograph showing white cores in halite with growth bands and slip bands. Finely dispersed anhydrite bands are next to very fine-grained halite. h) Photomontage of transmitted light image (with  $\lambda$ -plate) and reflected light image showing fluid inclusions at grain boundaries of fine-grained halite, polyhalite anhydrite and anhydrite band enriched with small anhydrite minerals.







690 **Figure 3: Overview of gamma decorated samples from Barradeel, Pieterburen, Zuidwending and Winschoten, together with maps of the interpreted microstructures. Reflected light images that were used for interpretation of grain boundaries are presented in Supplements 2. Anhydrite, polyhalite and gypsum layers were all mapped, but dispersed particles were mapped only partly as practicable.**



695 **Figure 4: a) Transmitted light salt core slab (Zuidwending) showing Kristallbrocken (KB), folded 3 mm thick anhydrite band in**  
**fine-grained halite matrix and unfolded, but boudinaged 3 mm thick anhydrite band next to Kristallbrocken. b) gamma irradiated**  
**transmitted light scans (samples KS-13A and B) location indicated in Fig. 4b) showing white cores and blue growth rims in fine-**  
**grained halite. c) Salt core slab photograph of Pieterburen slab and photo montaged transmitted light image of thick section**  
**showing Kristallbrocken (KB) with clear halite on the grain edges of Kristallbrocken grains. d) Transmitted light scan of gamma**  
700 **irradiated sample BS-A showing lighter blue cores and dark blue growth rims of fine-grained halite matrix.**

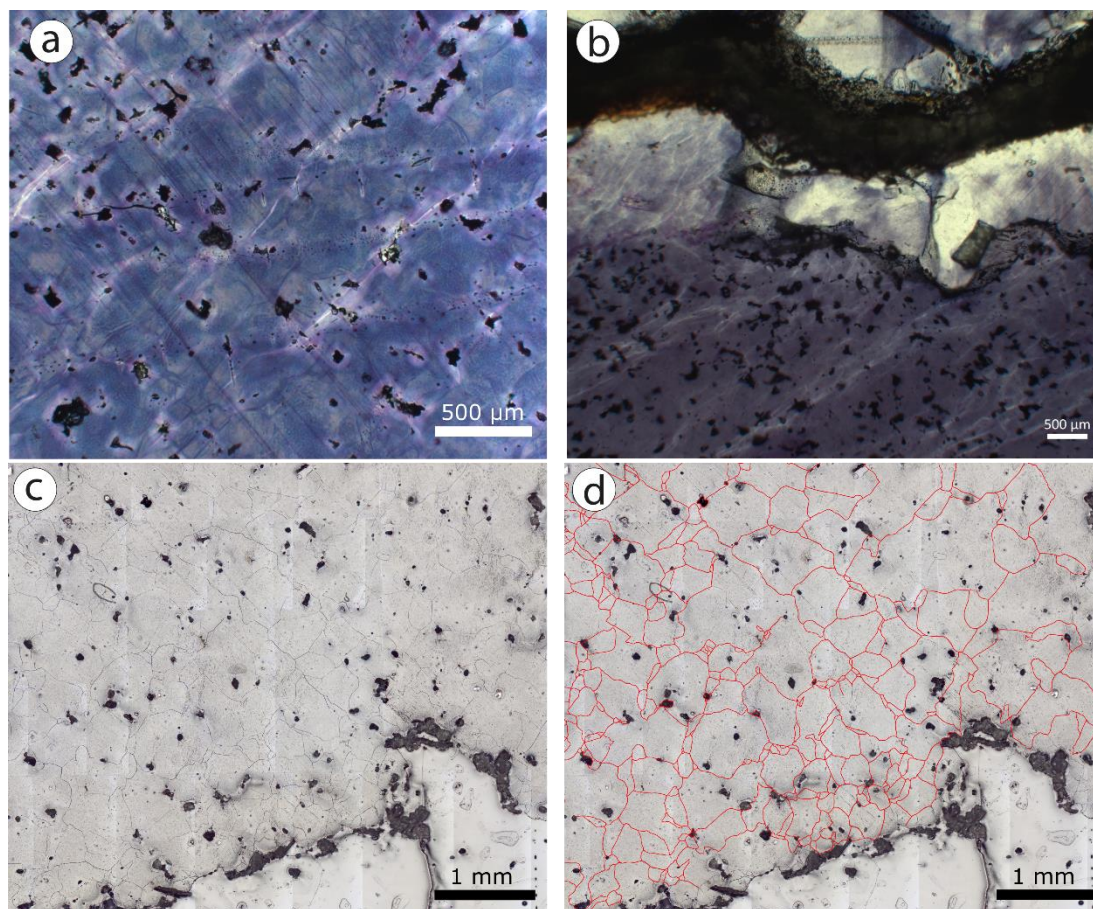


**Figure 5:** a) Transmitted light micrograph of gamma irradiated KS-08 (Winschoten) sample showing abundant dark inclusions in Kristallbrocken, slip bands and gamma decorated white subgrain boundaries. b) Transmitted light micrograph of gamma irradiated KS-05 (Winschoten) sample showing abundant dark inclusions, slip bands and gamma decorated white subgrain boundaries in Kristallbrocken next to anhydrite band and inclusion poor light halite in-between. c) Reflected light image of sample KS-08 (Winschoten) Kristallbrocken with abundant subgrains and mineral inclusions used for piezometry. Exact location indicated in Fig. 3, KS-08, s2. d) Digitized subgrain boundaries are an example of the data used for piezometry.

705



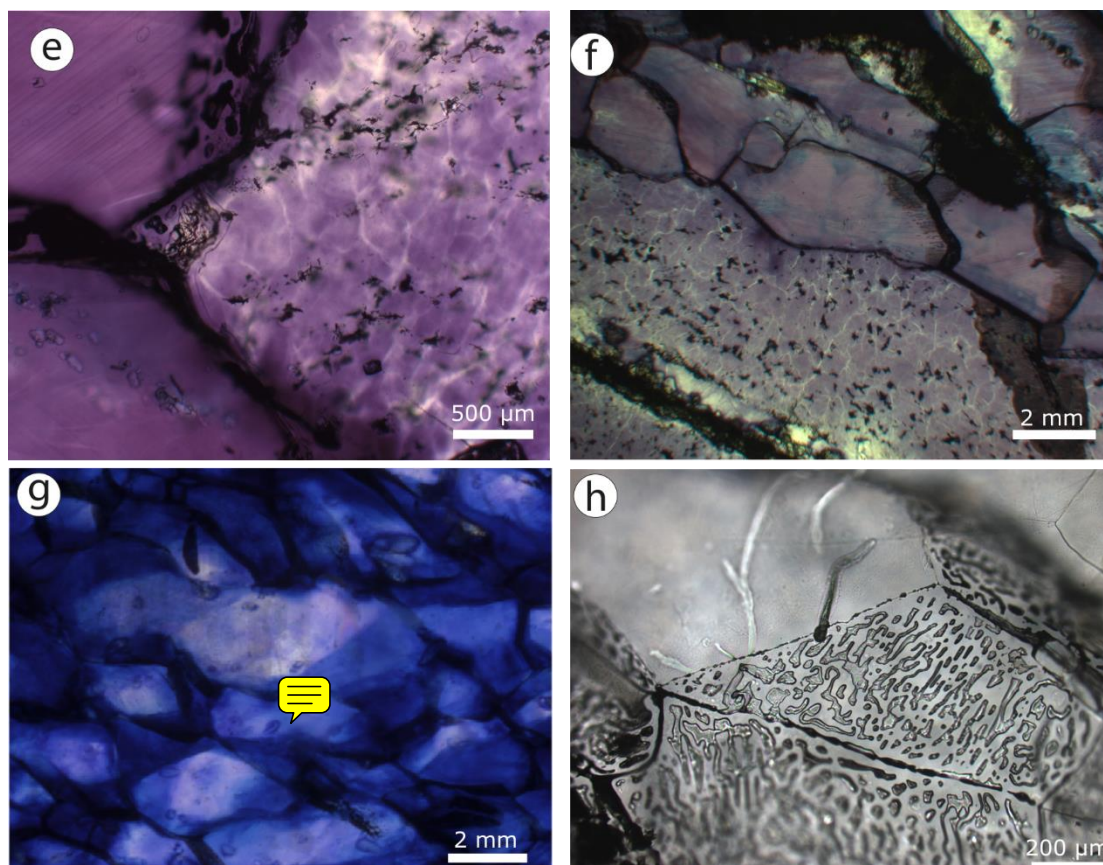


**Figure 5:** e) Transmitted light micrograph of gamma irradiated sample KS-13B (Zuidwending) showing Kristallbrocken grain with gamma decorated subgrains and abundant solid inclusions. Clear halite grain shows array of elongated anhydrite minerals parallel to grain boundary as well as abundant fluid inclusions at grain boundaries. f) Transmitted light micrograph of gamma irradiated Zuidwending sample KS-02 showing subgrain structures, abundant dark inclusions as well as clear elongated halite grains next to it. g) Transmitted light micrograph of gamma decorated halite grains showing light cores and directional overgrowth of elongated fine-grained halite in sample BS-B (Pieterburen). h) Transmitted light micrograph of thick section showing abundant fluid inclusions at fine-grained halite grain boundary of Pieterburen sample.

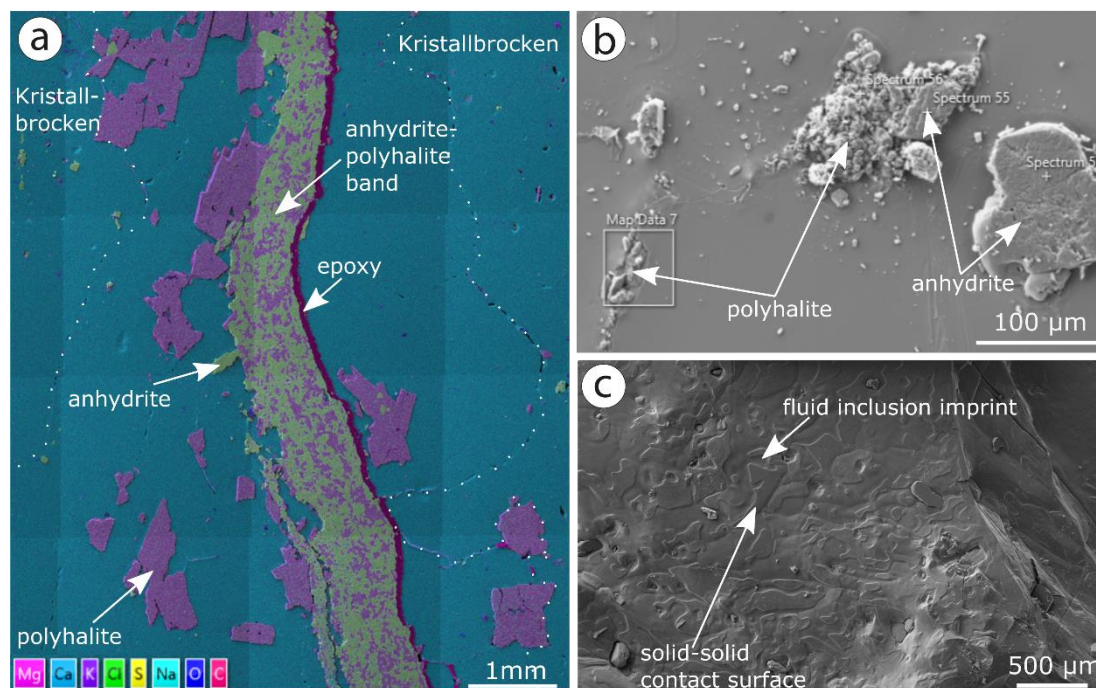


**Figure 6:** a) EDS map of KS-05 (Winschoten) showing anhydrite-polyhalite band, as well as Kristallbrocken with smaller anhydrite and polyhalite inclusions. b) SEM micrograph of polyhalite and anhydrite inclusions in fine-grained halite. c) SEM micrograph of Kristallbrocken broken along grain boundary showing fluid inclusion imprints and abundant Mg/K-sulfate inclusions.

720

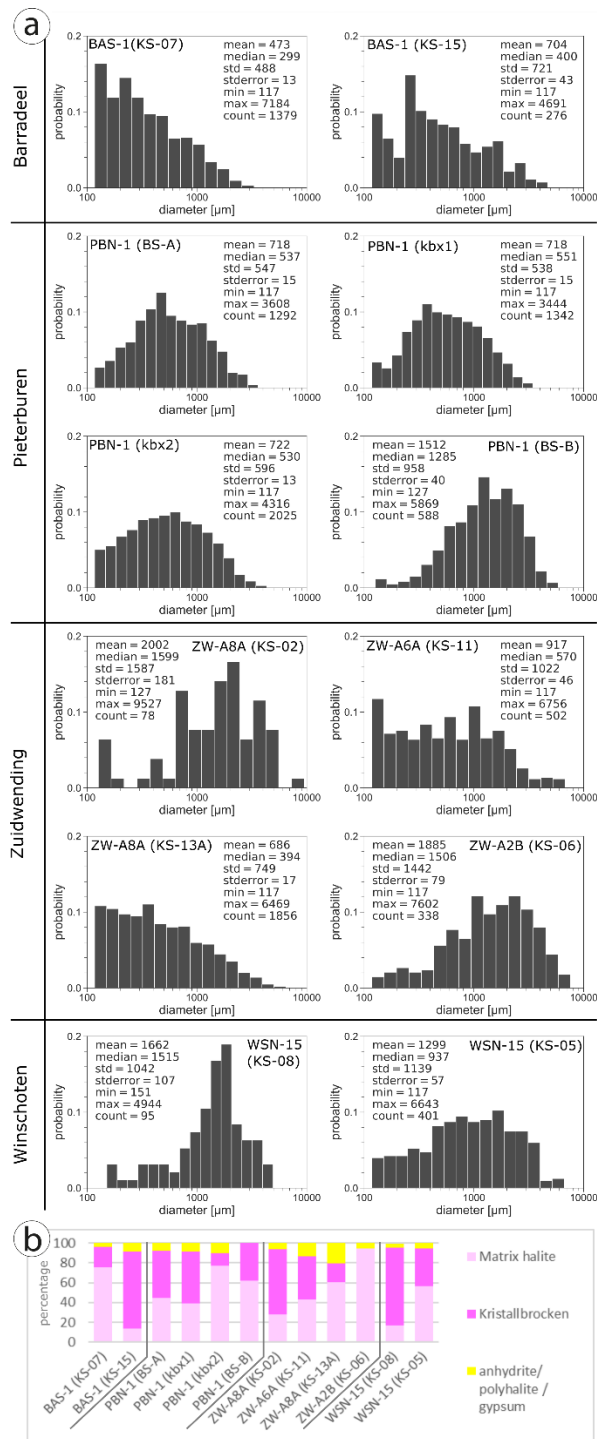
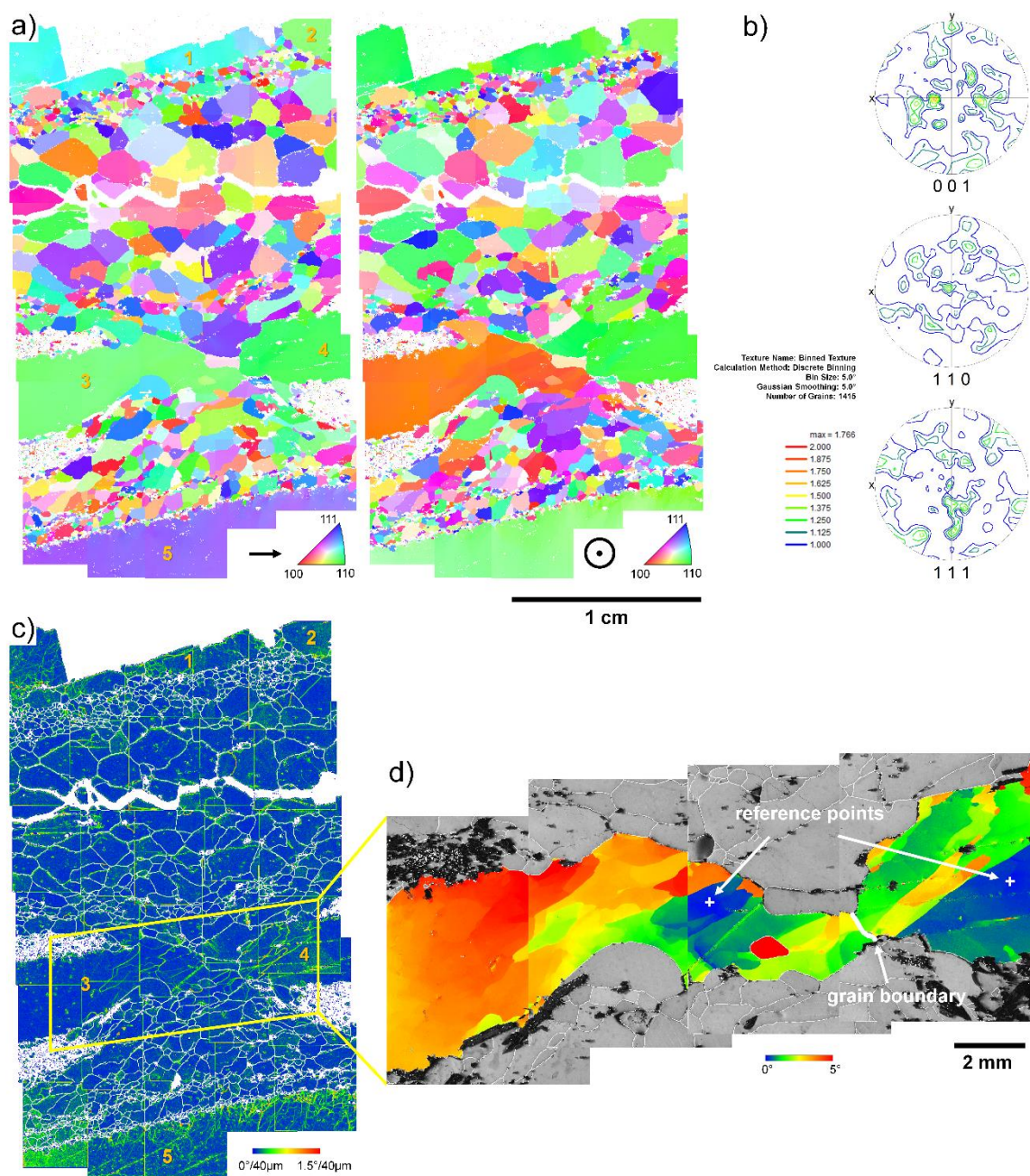


Figure 7: a) grain size histograms of fine-grained matrix halite for each sample presented in Figure 3 including statistical parameters. Grains smaller than 0.117 mm were not mapped due to image resolution. b) fractions of matrix halite, Kristallbrocken and anhydrite/ polyhalite and gypsum for each sample.





**Figure 8:** a) Inverse Pole Figure Maps for halite grains with large Kristallbrocken grains labelled 1-5. b) Pole figures of fine-grained matrix halite excluding 5 Kristallbrocken grains show no significant crystallographic preferred orientation (CPO). c) Kernel Average Misorientation (KAM) Map overlaid white low- and high-angle grain boundaries (misorientation > 5°). KAM shows subgrain-free matrix halite with few exceptions in large matrix halite grains, Kristallbrocken 1 and 5 with subgrains, and subgrains in boudin necks of Kristallbrocken 3 and 4, based on higher resolved EBSD measurements. Reference points for each of the two grains are indicated. Images a) and b) consist of 30 individual measurements, which due to image distortion under 70° tilt cannot be stitched perfectly. Therefore, in some cases an artificial separation of areas belonging to the same grain is visible.

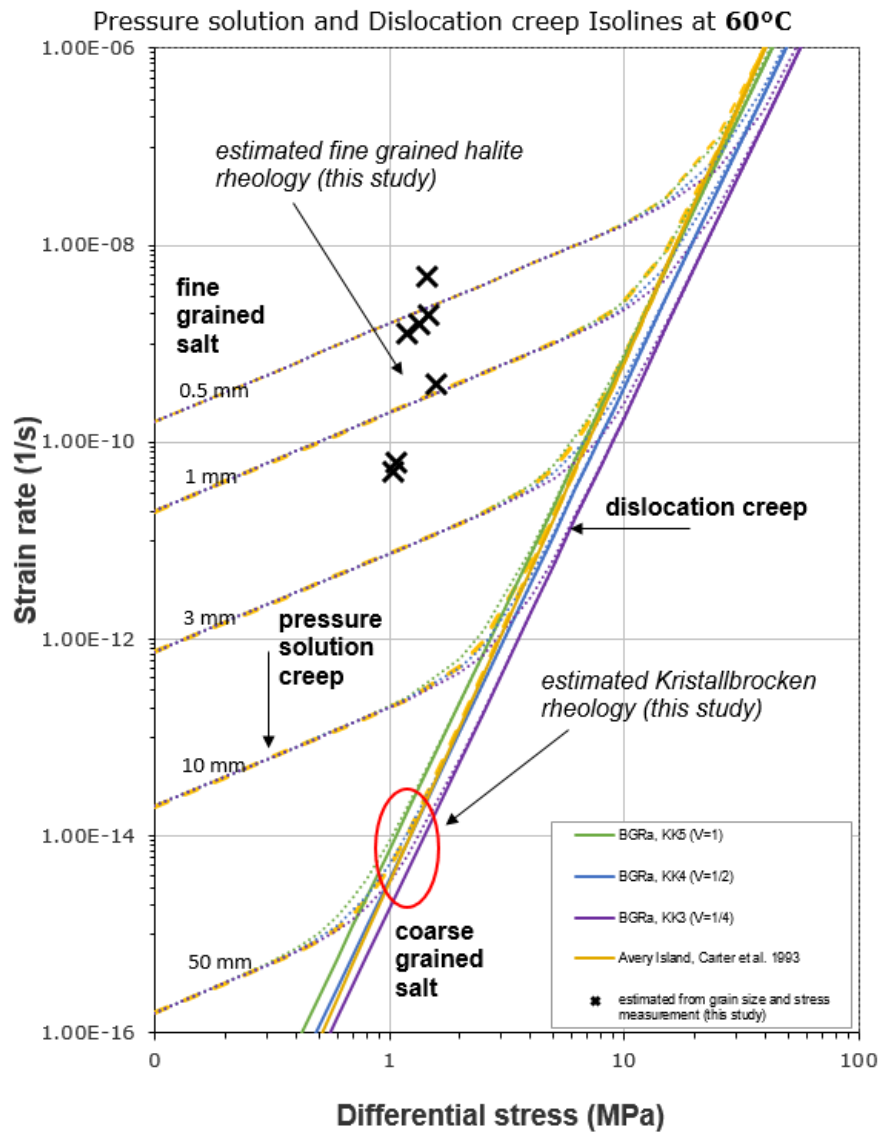
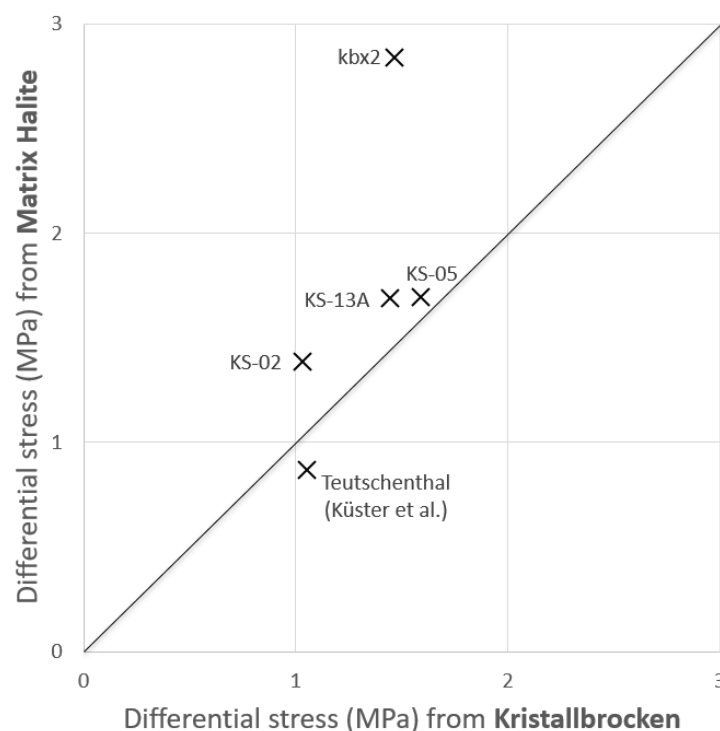


Figure 9: Differential stress vs strain rate diagram plotting selected flow laws at 60°C. BGRa KK='Kriechklassen' 5, 4 and 3 (Liu, W. et al., 2017) as well as Avery Island samples from (Carter et al., 1993) are included for dislocation creep. Dotted lines show combined pressure solution (Spiers et al., 1990) and dislocation creep flow laws for different halite grain sizes. Results from this study are plotted based on measured median fine-grained halite grain sizes (Fig. 7) and differential stresses from subgrain size piezometry of Kristallbrocken for each sample Supplement 2 and Table 1.



**Figure 10: Comparison of differential stresses measured in Kristallbrocken and matrix halite, for samples were both were available ( $\sigma = 107 \cdot (D^{-0.87})$ ,  $D$ = subgrain size, (Carter et al., 1993; Schlöder and Urai, 2005)). Measurements indicate comparable differential stresses for both halite types, but slightly lower values for differential stress in Kristallbrocken of this study. Differential stresses from Teutschenthal were measured based on micrographs presented in Küster et al. (2008) for matrix halite and Küster (2011) for Kristallbrocken and show comparable, slightly lower differential stresses.**



**Table 1 Differential stresses from subgrain size piezometry calculated with  $\sigma=107 \cdot D^{-0.87}$  (Supplement 2) after (Carter et al., 1993; Schlöder and Urai, 2005). Halite types KB=Kristallbrocken**

Location	Well and depth [m]	Sample and measured site	Halite type	mean subgrain diameter from area [ $\mu\text{m}$ ]	n	mean differential stress [MPa](95% confidence)	mean differential stress [MPa]
Pieterburen	(PBN-1) 588	kbx1 s1	KB	86.09	181	2.01 – 2.48	2.22
		kbx1 s2	KB	181.59	272	1.05 – 1.30	1.16
		kbx1 s3	KB	137.79	117	1.33 – 1.65	1.47
		kbx1 s4	KB	182.27	155	1.05 – 1.28	1.15
		kbx1 s5	KB	156.07	115	1.19 – 1.49	1.32
	(PBN-1) -	kbx2 s1	Matrix	64.87	52	2.49 – 3.30	2.84
		kbx2 s2	KB	131.98	467	1.45 – 1.62	1.53
		kbx2 s3	KB	126.82	496	1.49 – 1.69	1.58
		kbx2 s4	KB	217.19	115	0.89 – 1.12	0.99
Zuidwending	(ZW-A8A) 262	KS02 s3	Matrix	147.90	424	1.31 - 1.47	1.39
		KS02 s2	KB	259.48	304	0.79 - 0.92	0.85
		KS02 s1	KB	173.23	461	1.13 - 1.29	1.21
	(ZW-A6A) 599.4	KS11 s1	KB	379.63	106	0.55 - 0.69	0.61
		KS11 s2	KB	157.96	1205	1.26 - 1.36	1.31
	(ZW-A8A) 825.3	KS13A s8	Matrix	90.33	464	2.00 - 2.27	2.13
		KS13A s5	Matrix	142.68	516	1.32 - 1.56	1.43
		KS13A s3	KB	140.73	112	1.28 - 1.67	1.45
Winschoten	(WSN-15) 1659.5	KS06 s5	Matrix	103.91	32	1.61 - 2.27	1.89
		KS06 s7	Matrix	79.03	41	2.02 - 2.93	2.39
		KS08 s1	KB	252.52	262	0.80 – 0.95	0.87
	(WSN-15) 1661.5	KS08 s2	KB	196.88	601	1.01 – 1.16	1.08
		KS08 s3	KB	189.03	1007	1.06 – 1.18	1.12
		KS05 s4	KB	131.70	1210	1.47 – 1.60	1.53
		KS05 s1	KB	133.84	601	1.44 – 1.60	1.51
		KS05 s2	KB	86.83	235	2.02 – 2.42	2.20
		KS05 s3	KB	94.59	72	1.77 – 2.43	2.04
		KS05 s5	Matrix	117.29	58	1.50 – 1.96	1.69
Teutschen- thal, Germany	Fig. 2.10 (Küster, 2011) Fig. 7 (Küster et al., 2008)	KB	KB	188	68	0.90 – 1.26	1.05
		Matrix	Matrix	234	27	0.66 – 1.30	0.87